Delayed cone-opponent signals in the luminance pathway

Andrew Stockman UCL Institute of Ophthalmology, University College London, London, UK

G. Bruce Henning UCL Institute of Ophthalmology, University College London, London, UK

Sharif Anwar UCL Institute of Ophthalmology, University College London, London, UK

Robert Starba UCL Institute of Ophthalmology, University College London, London, UK

Andrew T. Rider UCL Institute of Ophthalmology, University College London, London, UK

Cone signals in the luminance or achromatic pathway were investigated by measuring how the perceptual timing of M- or L-cone-detected flicker depended on temporal frequency and chromatic adaptation. Relative timings were measured, as a function of temporal frequency, by superimposing M- or L-cone-isolating flicker on "equichromatic" flicker (flicker of the same wavelength as the background) and asking observers to vary contrast and phase to cancel the perception of flicker. Measurements were made in four observers on up to 35 different backgrounds varying in wavelength and radiance. Observers showed substantial perceptual delays or advances of L- and M-cone flicker that varied systematically with cone class, background wavelength, and radiance. Delays were largest for M-cone-isolating flicker. Although complex, the results can be characterised by a surprisingly simple model in which the representations of L- and M-cone flicker are comprised not only of a fast copy of the flicker signal, but also of a slow copy that is delayed by roughly 30 ms and varies in strength and sign with both background wavelength and radiance. The delays, which are too large to be due to selective cone adaptation by the chromatic backgrounds, must arise postreceptorally. Clear evidence for the slow signals can also be found in physiological measurements of horizontal and magnocellular ganglion cells, thus placing the origin of the slow signals in the retina—most likely in an extended horizontal cell network. Luminance-equated stimuli chosen to isolate chromatic channels may inadvertently generate slow signals in the luminance channel.

Introduction

The short- (S), middle- (M) and long- (L) wavelength-sensitive cone photoreceptors are responsible for our daytime chromatic and achromatic vision. Individually, each cone class generates a color-blind, "univariant" output signal that depends on the rate of quantal absorptions and therefore, by itself, confounds wavelength and intensity changes (e.g., Mitchell & Rushton, 1971). In the conventional model of the visual system, chromatic signals are extracted postreceptorally by differencing the cone signals in chromatic channels (L − M) or (S − [L+M]), which are relatively slow and respond better to low-frequency stimuli. If instead the cone signals are added together, as they are in the luminance channel (L + M), the sum also remains univariant and is therefore "achromatic" (e.g., Schrödinger, 1925; Luther, 1927; Walls, 1955; de Lange, 1958; Guth, Alexander, Chumbly, Gillman, & Patterson, 1968; Smith & Pokorny, 1975; Boynton, 1979; Eisner & MacLeod, 1980). Consequently, the luminance channel, like the cones, is color blind, so that flicker between two alternating lights, equated in luminance, that is detected solely by the luminance channel should appear steady (or "nulled"). In terms of cone excitations, alternating luminance-equated lights produce time-varying L- and M-cone signals that are equal and opposite in the luminance channel, so that their sum (L + M) remains constant. Such "flicker photometric" nulls, set at frequencies between 10 and 25 Hz (Troland, 1916; Ives, 1923), are the basis of the

Citation: Stockman, A., Henning, G. B., Anwar, S., Starba, R., & Rider, A. T. (2018). Delayed cone-opponent signals in the luminance pathway. *Journal of Vision*, *18*(2):6, 1–35, https://doi.org/10.1167/18.2.6.

https://doi.org/10.1167/18.2.6 Received October 3, 2017; published February 20, 2018 ISSN 1534-7362 Copyright 2018 The Authors

This work is licensed under a Creative Commons Attribution 4.0 International License.

Downloaded From: http://jov.arvojournals.org/pdfaccess.ashx?url=/data/journals/jov/936743/ on 02/20/2018

modern definition of luminance or luminous efficiency (Lennie, Pokorny, & Smith, 1993; Sharpe, Stockman, Jagla, & Jägle, 2005).

The measurements reported here are consistent with the notion of a *univariant* luminance channel, since above about 5 Hz, nulls are possible between any two near-threshold sinusoidally modulated stimuli. However, the two alternating stimuli must frequently be adjusted substantially away from opposing phase in order to null the perception of flicker (that is, away from the peaks of one sinusoidally-flickering light coinciding with the troughs of the other). This adjustment also changes the relative phases of the L- and M-cone signals away from opposite phase at the visual input. Substantial adjustments are inconsistent with the conventional model of the human visual system as being made up a "fast" luminance channel, which is silenced by luminance-equated flicker, and more sluggish chromatic channels, which are blind to high-frequency luminance-equated flicker. The motivation for the current series of experiments was to better understand why the conventional model fails.

One obvious cause of delays between cone signals is selective chromatic adaptation that can relatively advance either the L- or the M-cone signals within the luminance pathway. Although delays between L- and M-cone signals produced by chromatic adaptation can be large on long-wavelength backgrounds (the relative L- and M-cone phase delays can be calculated from the phase delay measurements of Stockman, Langendörfer, Smithson, & Sharpe, 2006), such delays are, in general, too small to account for the delays we find in our data. For example, the largest delay resulting from selective adaptation would occur on the longest wavelength background, which here was 658 nm, and which in terms of quantal catch is 1.09 $\log_{10}$ unit more effective for the L- than the M-cones (Stockman & Sharpe, 2000) and would produce phase delays of up to about 90° at 20 Hz. Shorter wavelengths would produce smaller delays. For example, at 440 nm the difference between L- and M-cone sensitivities is only 0.2 $\log_{10}$ unit, which is likely to produce phase delays of less than 20° at 20 Hz, whereas we found delays of about 180°. Instead, the relative cone delays must arise because of postreceptoral mechanisms operating in addition to photoreceptor adaptation. This work is focused on those mechanisms and how they arise.

The need to adjust alternating lights away from opposite (180°) phase in order to eliminate the perception of flicker and produce a null has been reported before. Early estimates of the necessary phase adjustments were relatively small, ranging from less than 9° away from 180° at 6 Hz and 4° at 14 Hz (de Lange, 1958), to less than 14° at frequencies between 20 and 55 Hz (Cushman & Levinson, 1983). Phase adjustments as large as 30° at frequencies below 9 Hz were reported by Walraven and Leebeek (1964), although their data may have been contaminated by rods (see also von Grünau, 1977). Much larger phase differences were reported by Lindsey, Pokorny, and Smith (1986) and by Swanson, Pokorny, and Smith (1987), who found phase delays between red and green flickering lights of nearly 180° at 2 Hz; i.e., flicker cancellation when the nominally opposed lights were almost in phase. These phase deviations from 180° fell rapidly with increasing frequency—to 0° by about 13 Hz.

We have used flicker cancellation experiments in which sinusoidally flickering lights that modulate single cone types were adjusted in phase and contrast to null sinusoidally flickering lights that mainly modulate the luminance channel. Thus, we have been able to obtain, relative to the luminance pathway, the phase and amplitude characteristics of signals generated by the three cone types (Stockman, MacLeod, & DePriest, 1991; Stockman, Montag, & MacLeod, 1991; Stockman & Plummer, 1994, 2005a, 2005b; Stockman, Plummer, & Montag, 2005). From these characteristics, we have identified several different sorts of cone input into the luminance channel, which we classify as "S," "M," or "L" according to the cone type from which they originate, "f" and "s" (fast and slow) according to their relative delay (phase shift) and/or their persistence (depending on the model, see below), and "+" and "–" according to whether the inputs have the same or are inverted in sign with respect to the fast (f) signal generated by the same cone type. So defined, seven distinct cone inputs appear to contribute to flicker nulls. They are: $+fL$, $+sL$, $-sL$, $+fM$, $+sM$, $-sM$, and $-sS$. In the Discussion we shall consider other work that is consistent with these inputs (Lindsey et al., 1986; Swanson et al., 1987; Smith, Lee, Pokorny, Martin, & Valberg, 1992; Stromeyer, Chaparro, Tolias, & Kronauer, 1997).

Here, we report unpublished measurements made previously at UC San Diego and recent measurements made at the UCL Institute of Ophthalmology (IoO) using the same optical system. The data are the phase delays for M- and L-cone isolating stimuli measured on a series of chromatic backgrounds that vary in wavelength and radiance.

Since much of this work has not been published in complete form until now, we need to put it into historical context. We first reported in abstract form in 1991 evidence for the slow and fast $+sM$ and $+fM$ signals, which destructively interfere near 15 Hz and reduce M-cone sensitivity on very bright red backgrounds (Stockman, Montag, et al., 1991), and followed that work with evidence for slow $-sM$ signals on less intense red fields three years later (Stockman & Plummer, 1994). We first reported evidence, also in abstract form, for the interactions between $+fM$, $+fL$,

Downloaded From: http://jov.arvojournals.org/pdfaccess.ashx?url=/data/journals/jov/936743/ on 02/20/2018

$-sM$, $+sM$, $-sL$, and $+sL$ in 2001 (Stockman, 2001). The results obtained on red backgrounds were eventually published in a series of four papers (Stockman & Plummer, 2005a, 2005b; Stockman, et al., 2005; Stockman, Montag, & Plummer, 2006). Our work measured on other chromatic backgrounds builds on the work of Stromeyer et al. (2000). Evidence for the $-sS$ signal was first reported in abstract form in 1987 (Stockman, MacLeod, & DePriest, 1987) and confirmed and characterized in subsequent publications (Lee & Stromeyer, 1989; Stockman, MacLeod, et al., 1991; Stockman, MacLeod, & Lebrun, 1993; Stockman & Plummer, 1998; Ripamonti, Woo, Crowther, & Stockman, 2009)

Our main motivation for publishing this work now is because we have obtained confirmatory measurements from two additional observers (SAA and RS) at the IoO, and we have formulated a physiologically plausible model that can account for the results. Two continuing difficulties are: first, identifying the origin of the substantial phase delays in the slow signals, and second, accounting for the prominent slow, *positive* cone signals that cannot easily be related to simple neural circuitry—in contrast to the slow, negative cone signals, which can be linked, at least in principle, to lateral inhibition.

In our current model (described in the Discussion), we account for the slow positive and slow negative cone signals in terms of the responses of an extended horizontal cell network produced by synergistic connections between neighboring cells through gap junctions. The overall sign of the slow cone signals produced by the whole network depends on the balance of the various slow signals from M- and L-cones with opponent surrounds feeding into the network. The balance will be affected by the relative number of L- and M-cones, the relative cone weights in the cone-opponent surrounds, and will be altered as chromatic adaptation to the steady background relatively suppresses the signals mediated by one or other cone type. On middle-wavelength background fields near 560 nm, we suppose that the M- and L-cones are balanced in sensitivity, so that the various slow signals in the horizontal cell network are roughly equal and thus cancel, substantially reducing the size of the slow signals relative to the fast ones. On long-wavelength backgrounds of low to moderate intensity, we suppose that the L-cones are suppressed relative to M-cones by the background fields, so that network signals through M-cones will predominate, thus favoring the $-sM$ and $+sL$ that travel though M-cones (see below). On intense long-wavelength backgrounds on which the L-cones are significantly bleached but the M-cones are not, and the background hue shifts towards yellow or green (Auerbach & Wald, 1955; Cornsweet, Fowler, Rabedeau, Whalen, & Williams, 1958), we suppose that the relative M-cone sensitivity losses start to exceed those of the L-cones, thus switching the balance to favor $-sL$ and $+sM$ signals through L-cones (Stockman & Plummer, 2005a). Similarly, on short-wavelength backgrounds, we suppose that the M-cones are relatively suppressed by the background fields, so that network signals through L-cones predominate, thus also favoring $-sL$ and $+sM$ signals.

These ideas and the data that support them are discussed in detail below. Crucially for our argument, evidence for these signals can be found in horizontal and ganglion cell recordings, which provide a firm physiological substrate (see Discussion).

We should also like to honor Daniel J. Plummer, who died on January 1st, 2006 in a cycling accident, and who was the main observer in this work, by dedicating this paper to his memory.

Methods

Apparatus

Measurements were made using a five-channel Maxwellian-view optical system illuminated by a 900-W Xe arc lamp with a 2-mm diameter exit pupil. Infrared and ultraviolet radiations were minimized by glass absorbing filters (Schott, Mainz, Germany). Maxwellian-view systems, which can be precisely controlled and calibrated, simultaneously image the illumination source in the pupil and the carefully positioned stimuli on the retina (Westheimer, 1966). Wavelengths were selected by the use of interference filters with full-width at half-maximum bandwidths of between 7 and 11 nm (Ealing Corporation, Holliston, MA, or Oriel, Stratford, CT). The radiance of each beam could be controlled by the insertion of fixed neutral density filters (Oriel) or by the rotation of circular, variable neutral density filters with a 3 $\log_{10}$ unit range (Rolyn Optics, Covina, CA). Temporal modulation was produced by pulse-width modulation of fast, liquid-crystal light shutters (Displaytech, Longmont, CO) at a carrier frequency of 400 Hz (which is much too fast to be resolved) so that the observers saw only the sinusoidal modulation of the pulse width. The liquid-crystal shutters had rise and fall times of less than 50 μs and the difference in transmission of the shutter in the primary test channel measured in situ between "on" and "off" was 70:1 at 410 nm, 140:1 at 440 nm, 230:1 at 470 nm and >300:1 at wavelengths longer than 500 nm. Consequently, the variability in attenuation with wavelength has a minimal effect of less than 3% on the modulation depth produced by the pulse-width modulation. With these shutters it was possible to simultaneously and independently modulate

Downloaded From: http://jov.arvojournals.org/pdfaccess.ashx?url=/data/journals/jov/936743/ on 02/20/2018

the intensities of four channels. The optical waveforms were monitored periodically using a PIN-10 photodiode (United Detector Technology, Hawthorne, CA) linear amplifier, and oscilloscope. In most of the experiments (see below), two of the channels were flickered in opposite phase and equated for one cone type, so that the flicker was silent for that cone type. The position of the observer's head was maintained by a dental wax impression mounted on a milling machine head.

Observers

Four male observers (AS, DJP, RS, and SAA) participated in these experiments. All had normal color vision, and were emmetropic. The color vision tests included the Ishihara test, City University test, the FM-100 test, and red-green Rayleigh matches. AS and DJP were experienced psychophysical observers, while RS and SAA were initially naïve but inevitably became highly experienced during the course of the experiment.

Stimuli

Sinusoidally flickering circular targets the diameters of which subtended 4° of visual angle were presented in the center of a circular, steady, 9° background field. Fixation was central. The monochromatic background field had one of ten wavelengths: 410, 440, 469, 491, 520, 550, 578, 600, 633, and 658 nm (or 650 nm for DJP), and one of four or more radiance levels, which we specify in $\log_{10}$ quanta s^{-1} deg^{-2}. The levels are tabulated in Tables A1 through A4 in the Appendix for observers DJP, SA, RS, and AS, respectively. For ease of summary, the radiance levels were separated into four groups, which are referred to as A: Low levels (1.42 – 1.98 log trolands, "Td"), B: Moderate levels (2.64 – 3.09 log Td), C: High levels (3.83 – 4.33 log Td) and D: Very high or bleaching levels (5.13 – 5.40 log Td). The 410-nm retinal illuminances (Td) are lower than those for other wavelengths in the A and B ranges because photopic Td underestimates luminous efficiency at short-wavelengths (see, for example, Sharpe, Stockman, Jagla, & Jägle, 2011). The 650-nm troland values in the D range are lower for SAA and RS because the system at UCL could not produce the high intensity that was possible at UC San Diego. The levels were originally chosen to allow us to minimize the number of background conditions but to be able to vary the M-cone and L-cone adaptation levels roughly independently of one another. Our results suggest, however, that the important background property determining the form of the phase characteristics was the *difference* in M- and L-cone excitation.

Three types of targets were used: M-cone isolating, L-cone isolating, and equichromatic targets. The equichromatic targets were so called because they had a wavelength very close to that of the background. Cone-isolating targets, created by "silent substitution," were produced by alternating two monochromatic sinusoids the intensities of which were matched for the cone type the response of which we wished to exclude. When the two sinusoids were modulated at the same frequency but in opposite phase, they generated the required cone isolating signal. Thus the M-cone isolating targets were a sinusoidally alternating pair of 540- and 650-nm lights whose intensities were equated for L-cones, while the L-cone isolating targets were sinusoidally-alternating 650- and 550-nm lights equated for M-cones. We initially used the Stockman and Sharpe (2000) cone fundamentals to equate pairs of lights for the different cone types. Thus, for M-cone isolation the 650-nm target in $\log_{10}$ quanta s^{-1} deg^{-2} was set to be 0.81 $\log_{10}$ unit more intense than the paired 540-nm target (to equate the L-cone responses), whereas for L-cone isolation the 650-nm target in $\log_{10}$ quanta s^{-1} deg^{-2} was set to be 1.87 $\log_{10}$ units more intense than the paired 550-nm target (to equate for M cones). From measurements and controls carried out on observers DJP and AS over many years, we know those values gave good M- and L-cone isolation for them. The same values for L-cone isolation produced comparable L-cone phase delays for SAA and RS. However, the values for M-cone isolation gave significantly reduced M-cone phase delays for SAA and RS compared to DJP and AS. This result led to a series of control experiments in which the relative radiance of the 650- and 540-nm lights was varied and the "M-cone" phase delays remeasured. We found that for SAA, the 650-nm target had to be 0.95 $\log_{10}$ unit more intense than the 540-nm target to produce M-cone phase delays similar to those of DJP and AS, while for RS the target had to be 0.90 $\log_{10}$ unit more intense. These differences are consistent with an L-cone polymorphic spectral sensitivity shift of 3 to 5 nm towards longer wavelengths for observers with serine at position 180 of the L-cone opsin gene compared to those with alanine at position 180 (e.g., Merbs & Nathans, 1992; Kraft, Neitz, & Neitz, 1998; Sharpe et al., 1998). We know that AS has serine at position 180 (Jeremy Nathans, personal communication), so we can reasonably assume that DJP also has serine at position 180 but that both SAA and RS probably have alanine there (unlike AS, however, they have not been genotyped).

Even with the optimal radiances for silent substitution, retinal inhomogeneities over the central 4° mean that the silent substitution is unlikely to be *perfect* over the whole 4° diameter target. Nevertheless, we should expect the stimuli predominantly to modulate the wanted cone.

Downloaded From: http://jov.arvojournals.org/pdfaccess.ashx?url=/data/journals/jov/936743/ on 02/20/2018

For each background condition, the radiance of the target or target pair was adjusted so that at 92% contrast the M-cone isolating, L-cone isolating, or equichromatic flicker was just visible at 25 Hz for the "Medium" to "Very High" background radiances or at 15 Hz for the "Low" background radiances.

On the most intense long-wavelength backgrounds, an auxiliary 410-nm steady background was superimposed on the background field to minimize any possibility that 540- or 550-nm flicker was detected by S-cones. Observers light adapted to test and background fields for at least 3 min prior to any data collection.

To suppress the rods at the lower background radiances, we bleached them by presenting DJP with a 510 nm background of 12.22 $\log_{10}$ quanta s^{-1} deg^{-2} (or 6.56 $\log_{10}$ scotopic Td) for 3 s (a bleach of 7.03 $\log_{10}$ scotopic Td-s) or by presenting SAA and RS with a 510 nm background of 11.90 $\log_{10}$ quanta s^{-1} deg^{-2} (or 6.24 $\log_{10}$ scotopic Td-s) for 7 s (a bleach of 7.08 $\log_{10}$ scotopic Td-s). Both bleach more than 99% of the rod photopigment (e.g., Pugh, 1988). Measurements were made between 3 and 10 min during the cone plateau following the bleach.

The sinusoidally flickering stimuli were varied in modulation and in phase. The cone ripple ratio or depth-of-modulation, m—here called modulation for simplicity—was defined as the conventional Michelson contrast:

$$m = \frac{I_{max} - I_{min}}{I_{max} + I_{min}}, \quad (1)$$

where I_{max} and I_{min} are the maximum and minimum radiances, respectively, of the sinusoidally flickering stimuli. The cone modulations were then calculated using the Stockman and Sharpe (2000) cone fundamentals.

Procedures

Observers interacted with the computer by means of eight buttons, and received feedback and instructions by means of tones and a computer-controlled voice synthesizer. The ability to give observers simple instructions during the course of the experiments enabled us to adopt complex testing procedures, even with relatively naïve observers.

Phase delays were measured using a simple extension of flicker photometry: One stimulus was a cone-isolating, matched pair of targets that together generated a flicker signal predominately in either M-cones or L-cones. The other stimulus was a flickering target of approximately the same wavelength as the background to produce the equichromatic flicker. Prior to the observers varying the phase between the equichromatic and cone-isolating stimuli to produce a flicker null, one stimulus was set to zero modulation, while the observer adjusted the modulation of the other stimulus until its flicker was just above threshold (typically about 0.20 $\log_{10}$ above threshold). This was done separately for both stimuli. Next, the two types of stimuli were flickered together, beginning in counterphase (i.e., 180° out-of-phase), and the observer's task was to find a flicker null by adjusting their relative phase and modulation. Observers could advance or retard the phase in steps of either 2° or 10°, and they could reverse the relative phase of one of the stimuli by 180°. This last option proved helpful in finding the cancellation phase quickly. If the observers were close to the nulling phase, the perception of flicker would increase markedly when the phase was reversed, whereas if they were 180° away from the nulling phase, the perception of flicker would decrease with the phase reversal. In contrast, if the observers were off by ±90°, the perception of flicker would not change appreciably when the phase was reversed. At any time during the phase settings, observers could adjust the modulation of either flickering stimulus to improve the flicker null. If the null covered an extended range of phase delays, which was usually the case if one of the two signals was weak, observers were instructed to set the middle of the range.

Except where noted, all data points are averaged from three or four settings made on three or four separate runs.

The visual stimulus, focused in the plane of the pupil, was the only visible light source for the observers in an otherwise dark room, and observers used their right eyes for observation; their left eyes were covered. The image of the source in the plane of the observers' pupils was always less than the minimal pupil size so that retinal illumination was not affected by pupil size.

Calibration

The radiant fluxes of test and background fields were measured at the plane of the observer's entrance pupil with a UDT Radiometer (Gamma Scientific, San Diego, CA) that had been calibrated by the manufacturer against a standard traceable to the National Bureau of Standards. The accuracy of this instrument was checked by cross-calibration with other devices calibrated against national standards in Germany and in the US. Neutral density filters, fixed and variable, were calibrated in situ for all test and background wavelengths. Particular care was taken in calibrating the interference filters: A spectroradiometer (EG&G or Gamma Scientific, San Diego, CA) was used to check for any side-band leaks, and to measure the center wavelength and the bandwidth at half amplitude of each interference filter in situ.

Downloaded From: http://jov.arvojournals.org/pdfaccess.ashx?url=/data/journals/jov/936743/ on 02/20/2018

Results and model fits

Phase measurements

Phase delay measurements are shown in Figure 1 for observer DJP, Figure 2 for SAA, and Figure 3 for RS, and Figure 4 for AS. Each row has the background wavelength shown to the right of the row, and each column has the radiances ranging from low (A) to high (D) labelled at the top of the columns.

Each panel shows the phase delay (degrees) of the M-cone flicker (green circles) or the L-cone flicker (red squares) required to null an equichromatic target as a function of frequency (Hz, linear scale). The phase lag is measured relative to the signal produced by equichromatic flicker with 0° indicating the two signals are in *opposite* phase and would therefore cancel on the basis of a conventional model and if there were no slow signals. We assume that equichromatic flicker generates predominantly $+fL$ and $+fM$ signals. It is important to note that adaptation will change the relative phase of the $+fM$ and $+fL$ signals (Stockman, Langendörfer, et al., 2006), particularly for long- and short-wavelength backgrounds that selectively adapt the L- or M-cones. As we point out below, evidence for this can be seen in the data, but the effects are small relative to the delays of roughly 29 ms between the slow and fast signals.

For convenience, we plot the phase delays in the range −180° to 360° (rather than over a 360° range). This allows us to plot all the phase characteristics as continuous functions: those dominated by $+sM$ or $+sL$ plot between 0° and 360° and those dominated by $-sM$ or $-sL$ plot between −180° and +180°.

The phase data shown in Figures 1 through 4 are complex, but all the observers show the same characteristic variations with background wavelength and radiance. The curves in each panel are related to the model to which we now turn.

Time-delay representations

To help describe and categorize the varying phase delay characteristics and to make it easier to understand them, we introduce, in Figure 5, two vector diagrams and predicted phase delays that illustrate how the "fast" and the delayed "slow" signals interact (see also Stockman & Plummer, 2005b, 2005a; Stockman et al., 2005). Thus, we are combining Results and Discussion in this section.

In the representations shown on the right of Figure 5, we assumed that the M- and L-cone signals are the resultants (thick black vectors of amplitude r) of the vector addition of the slow (cyan vectors, amplitude s) and fast signals (orange vectors, with amplitude f); the slow signal is delayed in time by Δt. The time delay is represented here by the phase delay $\Delta\theta$. (Note that we are now using the symbols s and f to play the additional role of denoting the amplitudes of the slow and fast signals.) The upper panels show the case where the slow and fast signals have the same sign, the lower panels where they have opposite signs. The vector addition of the slow and fast vectors produces the resultant (thick black) vector with amplitude r and phase delay ϕ where the phase delay ϕ is measured relative to the fast (horizontal orange) vector. It is this phase delay that we measure in our experiments because the flicker of the equiluminant vector that is nulled is determined almost exclusively by the fast vector. For a given background condition the whole triangle, by convention, rotates counter clockwise at a rate of $360\nu/2\pi$ degrees per second where ν is the flicker frequency in Hz. Because of this convention, delays produce phase delays that are represented by clockwise rotations. The phase delay, $\Delta\theta$ between the slow and fast signals, in degrees, is given by:

$$\Delta\theta = 0.36\nu\Delta t, \quad (2)$$

where Δt is the time delay in ms, and ν is again the frequency of the flicker in Hz (note that we use ν for frequency to avoid confusion with our notation of f for the fast cone signals).

Equation 2 shows that for a fixed time delay, Δt, the corresponding phase delay, $\Delta\theta$, between the slow and fast signals increases with frequency. This means that the slow vector rotates clockwise relative to the fast vector as frequency increases. The resultant vector, then, varies in length or amplitude, r, and phase delay, ϕ, as the slow vector changes. In general, the phase delay of the resultant cone signal, ϕ is given in degrees by

$$\phi = \arctan\left(\frac{\frac{s}{f}\sin\Delta\theta}{1+\frac{s}{f}\cos\Delta\theta}\right). \quad (3)$$

It is the angle ϕ that we measure in our experiments.

For convenience, we normalize the lengths of the slow and fast vectors such that $\hat{s} = s/(s+f)$ and $\hat{f} = f/(s+f)$. Since $\hat{f} = 1 - \hat{s}$, we use only $\hat{s}$ as the parameter that differentiates the curves in the figures on the left of Figure 5 where $\hat{s}$ varies from 0 (all fast signal) to 1 (all slow signal).

The curves in the left-hand panels of Figure 5 correspond to the vector diagrams and show phase delay, ϕ, as a function of frequency (Hz). The parameter in both cases is the normalized amplitude of the slow component, $\hat{s}$, which varies in 0.1 steps from 0 (no slow signal, producing the limiting orange horizontal line at 0° phase delay) to 1 (no fast signal, producing the limiting cyan straight line that passes through the origin with constant slope of $0.36\Delta t$ degree per Hz given Δt in ms). For the simulations in Figure 5,

Downloaded From: http://jov.arvojournals.org/pdfaccess.ashx?url=/data/journals/jov/936743/ on 02/20/2018

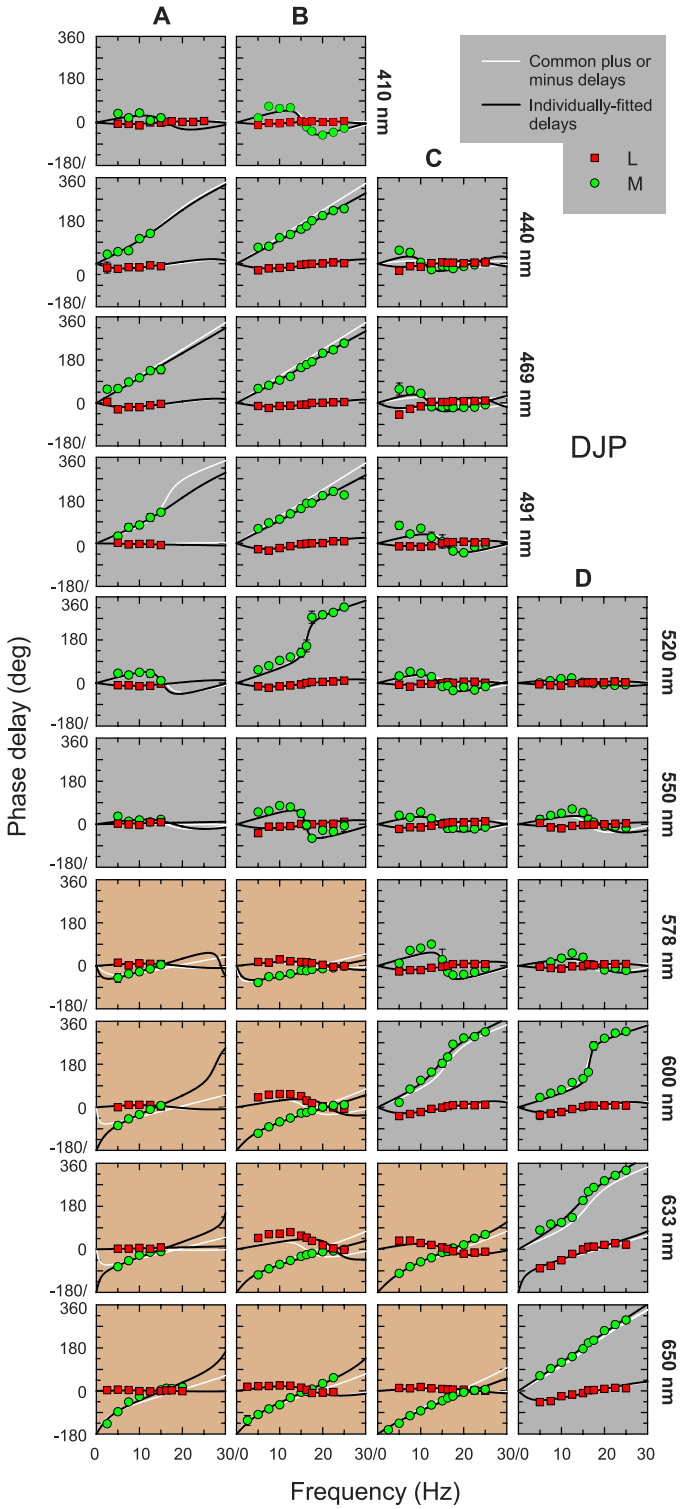

Figure 1. Each panel show measured phase lags (degrees) for observer DJP as a function of frequency (Hz). The panels in each row correspond to the background wavelength (nm) indicated to the right, while each column represents a different intensity: (A) Low Levels, (B) Moderate Levels, (C) High Levels, and (D) Very high levels. Thirty-five different background conditions were used. (The conditions are summarized in Tables A1 through A4 in the Appendix). The red symbols represent data from L-cone isolating flicker, and the green symbols, M-cone isolating flicker. The black and white smooth curves fitted to the data in each panel are predictions from models discussed in the text. The panels with gray backgrounds correspond to conditions under which the slow signals in the models are predominately $+sM$ and $-sL$, and the brown panels to conditions under which the slow signals are predominantly $-sM$ and $+sL$ (see text for details).

Downloaded From: http://jov.arvojournals.org/pdfaccess.ashx?url=/data/journals/jov/936743/ on 02/20/2018

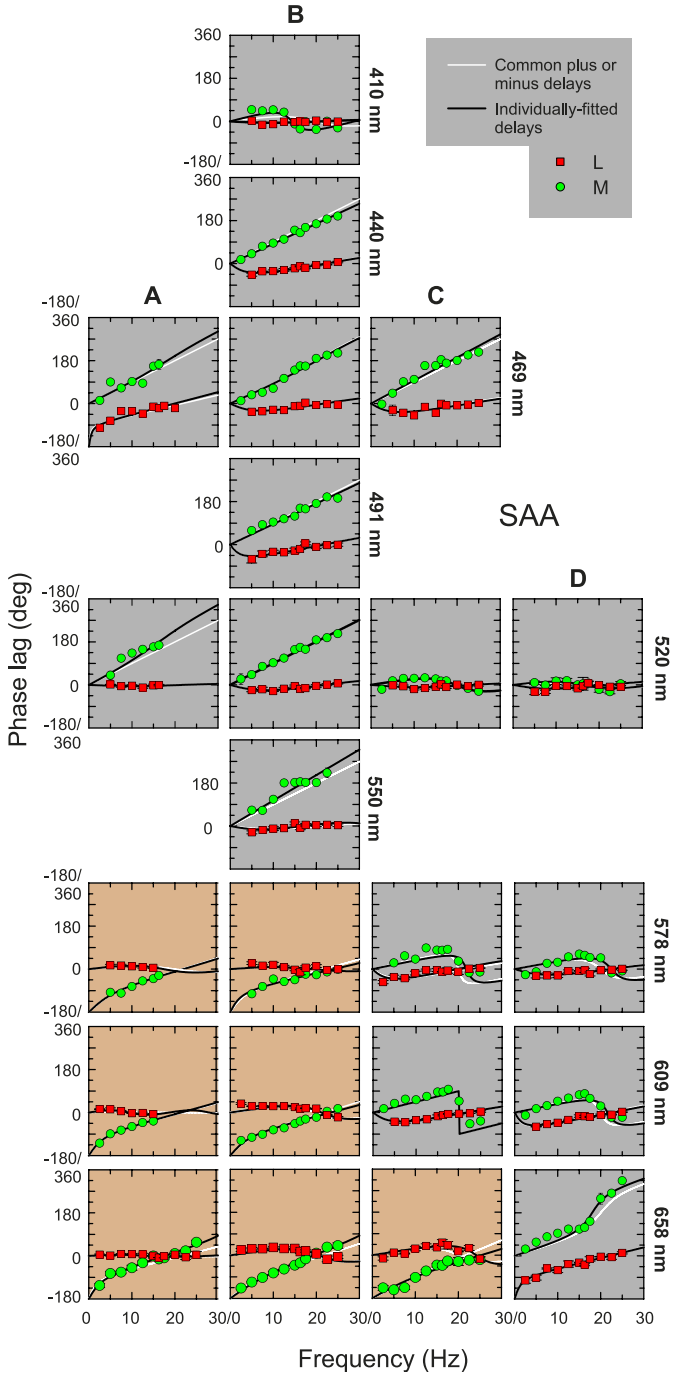

Figure 2. Details as for Figure 1 but for observer SAA.

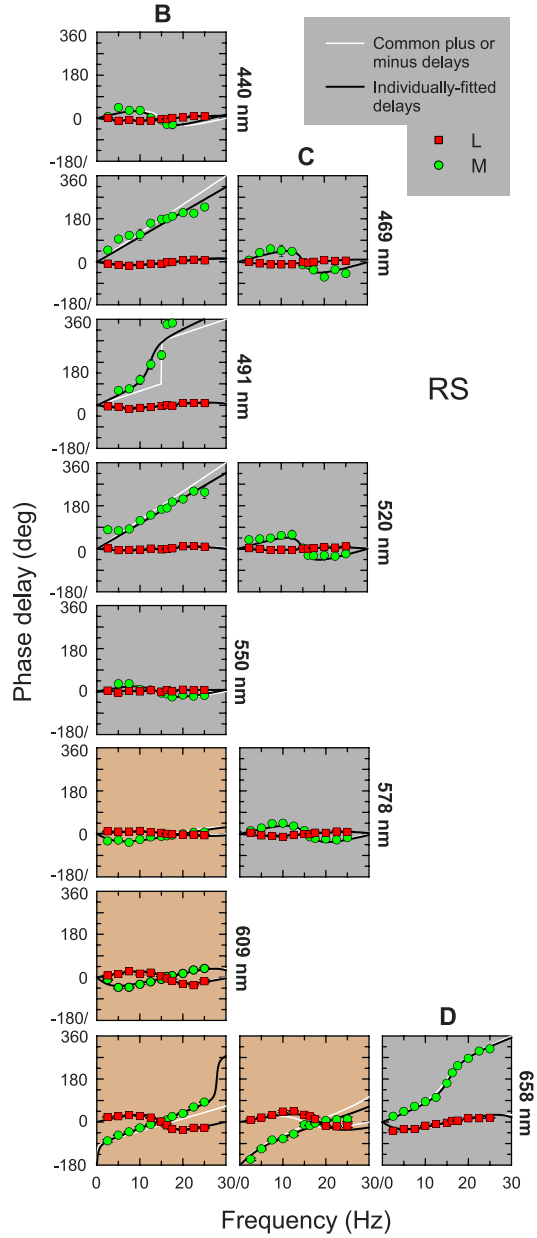

Figure 3. Details as for Figure 1 but for observer RS.

the value of the delay between the slow and fast signals, Δt, has been set at 29 ms, which is approximately the mean best-fitting value found across observers (see Figure 7), and from Equation 2, can be seen to correspond to a phase delay of 180° near 17 Hz. The pattern of phase delays with changes in $\hat{s}$ is a straightforward consequence of Equations 2 and 3 and the vector diagrams on the right of the figure.

The upper panel (A) of Figure 5 shows the case when the slow and fast signals have the same sign. However, an important feature of our representation is that the slow signals can have the opposite sign from the fast signal, as illustrated in the lower panel (B). Changing the sign of the slow signal is equivalent to either an additional phase advance or delay of 180°, as shown in the vector diagram in (B), so $\Delta\theta$, in degrees becomes:

$$\Delta\theta = 0.36\upsilon\Delta t - 180. \quad (4)$$

The patterns on the left are the consequence of Equations 3 and 4 and the vector diagrams. Note that implicit in this representation is the assumption and simplification that neither Δt nor $\hat{s}$ vary with frequency, which means that the *shapes* of the temporal contrast-sensitivity functions for the slow and fast signals are identical. In other models, we allowed a low-pass filter

Downloaded From: http://jov.arvojournals.org/pdfaccess.ashx?url=/data/journals/jov/936743/ on 02/20/2018

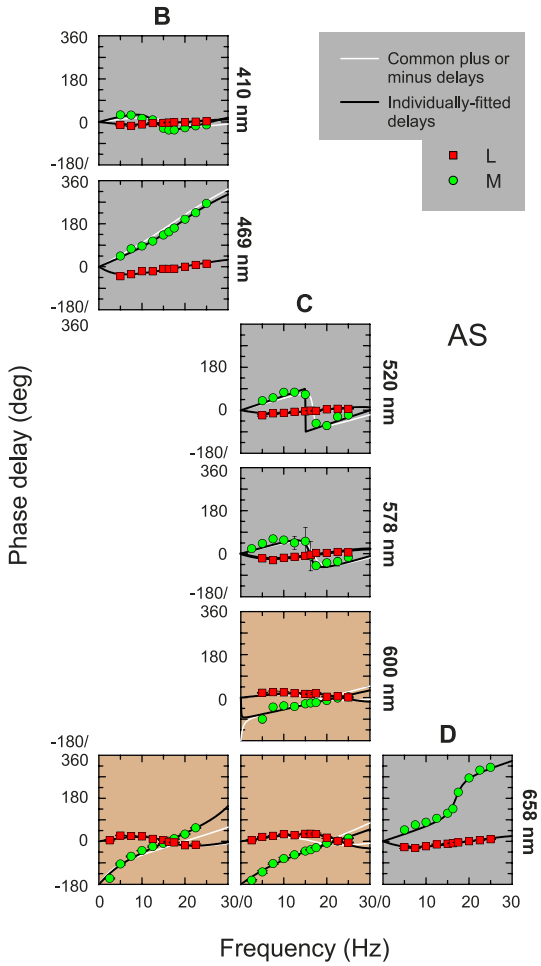

Figure 4. Same as Figure 1 but for observer AS.

in the slow pathway, which decreases s relative to f as frequency increases (see below).

The primary determinants of the form of the phase characteristics seen in both panels of Figure 5 are first $\hat{s}$, and in particular whether $\hat{s}$ is greater or less than 0.5 (i.e., which of s or f is greater; see Equation 3), second Δt, and third the sign of the slow signal, and in particular the frequencies over which the slow and fast signals destructively or constructively interfere. In the simulations of Figure 5, complete destructive interference of slow and fast signals of equal amplitude would occur near 17 Hz for the slow positive signal and near 0 and 34 Hz for the slow negative signal. Near those frequencies there can be characteristically abrupt changes of up to 180° in phase delay. On the other hand, the maximum *constructive* interference occurs near 0 and 34 Hz for the slow positive signal and 17 Hz for the slow negative signal.

As can be inferred from the vector diagrams in Figure 5, the interaction between the slow and fast signals affects the magnitude as well as the phase of the resultant. As we have shown before, however, the phase measurements are much more diagnostic for inferring the nature of the underlying signals and their interactions than modulation-sensitivity data (Stockman & Plummer, 2005b, 2005a; Stockman et al., 2005). Consequently, in this work we have measured phase delays.

Basic model fits

Our strategy has been to look for the patterns of phase delays in our data comparable to those seen in Figure 5 from which we can infer the identity of the underlying cone signals, their relative strengths, signs, and delays. Figure 6 illustrates two examples of this process. The graphs and diagrams in the upper panels (A) of Figure 6 illustrate stimuli used for M-cone phase measurements made on the 469-nm, medium-radiance, B-level-background and the results for observer AS. The stimuli are shown on the right: superimposed on a steady 469-nm background (blue cylinder) were (a) a nearly equichromatic 469-nm sinusoidally modulated light (top blue disk) and (b) an L-cone equated pair of 540 and 650-nm targets (middle red and green disks) that, when sinusoidally-modulated in opposite phase, generated the M-cone-isolating sinusoidal modulation. At each frequency, the observer adjusted the relative modulation and phase of the 469-nm and the M-cone-isolating flicker to null the perception of flicker.

The green circles in the upper left graph show the phase adjustments *away* from opposite phase that were required to produce the null. The settings tend towards 0° with decreasing frequency, which means that at low frequencies the stimuli nulled each other when they were in opposite phase. However, the settings reach 180° near 18.6 Hz, which means that at that frequency the stimuli had to be in the same phase to null each other.

The graphs and diagrams in the lower panels (B) of Figure 6 show the results and stimuli also for M-cone phase measurements but made on the high-radiance, 658-nm C-level-background as shown on the lower right. Superimposed on the 658-nm background were (a) a nearly equichromatic 656-nm sinusoidally modulated light and (b) again an L-cone equated pair of 540 and 650-nm targets that together generated an M-cone modulation. The green circles in the lower left graph show the phase adjustments required by AS to produce a null. Under these conditions, the settings tend towards −180° with decreasing frequency. A setting of −180° (as for +180° in the previous example) means that the observer adjusted the stimuli to be in the same phase to null. The setting of 0° near 22 Hz means that at 22 Hz, the stimuli nulled each other when they were in opposite phase (i.e., no phase adjustments away from opposite phase were needed).

The simulations shown by the continuous lines in Figure 6 illustrate how the phase characteristics

Downloaded From: http://jov.arvojournals.org/pdfaccess.ashx?url=/data/journals/jov/936743/ on 02/20/2018

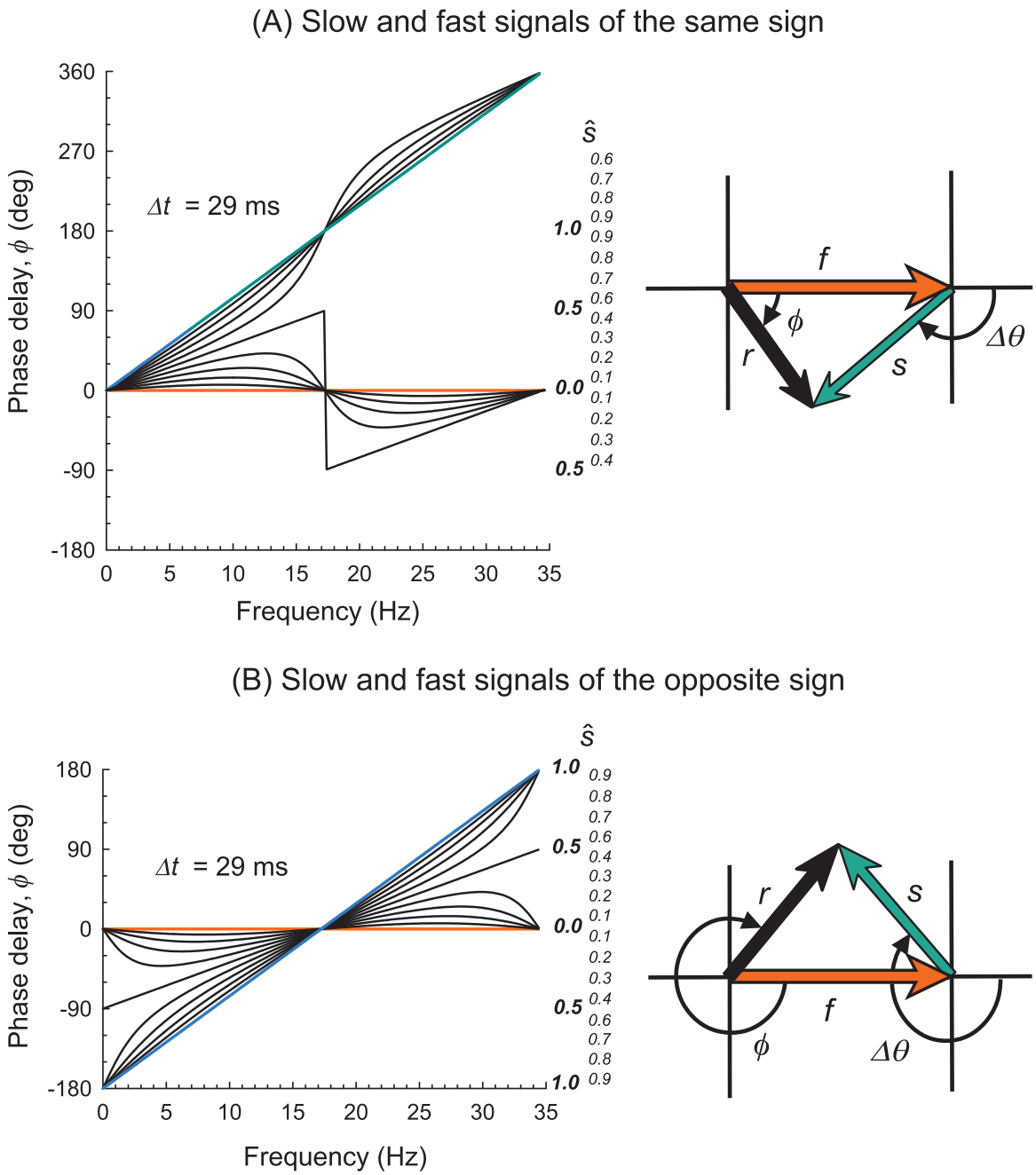

Figure 5. Right-hand figures: vector diagrams. The cone-isolating target is assumed to generate a fast cone signal, (horizontal orange arrow of length *f*), and a slow cone signal (cyan arrow of length *s*) separated by the phase delay of the slow signal, $\Delta\theta$. The fast and slow vectors combine to produce the resultant cone signal (black arrow of length *r*) The resultant has a phase delay, ϕ, relative to the fast signal. It is this delay we determine by the flicker null with the equichromatic target (which is assumed to generate only fast signals). Thus, the phase delay, ϕ, is directly measured in our experiments. The diagram in the upper panel (A) shows slow and fast signals of the same sign. The diagram in the lower panel (B) shows slow and fast signals of opposite sign, so that in the latter case the slow signal is effectively delayed (or advanced) by an extra 180°. The upper and lower left-hand panels correspond to the upper and lower vector diagrams, respectively. They show the phase delay of the resultant ϕ (degrees) as a function of frequency (Hz). The different curves in each panel show the resultant phase delays for different ratios of *s*/*f*—specified as a normalized slow weight $\hat{s}$, where $\hat{s} = s/(s+f)$ for slow and fast signals of the same (upper) or opposite (lower) signs. For these graphs there was a fixed time delay, Δt, between the slow and fast signals of 29 ms—close to the mean value in our basic model (see text). The horizontal orange line corresponds to a zero-amplitude slow component, $\hat{s} = 0$, the cyan line corresponds to a zero amplitude fast component, $\hat{s} = 1$ with a slope determined by the 29-ms delay.

Downloaded From: http://jov.arvojournals.org/pdfaccess.ashx?url=/data/journals/jov/936743/ on 02/20/2018

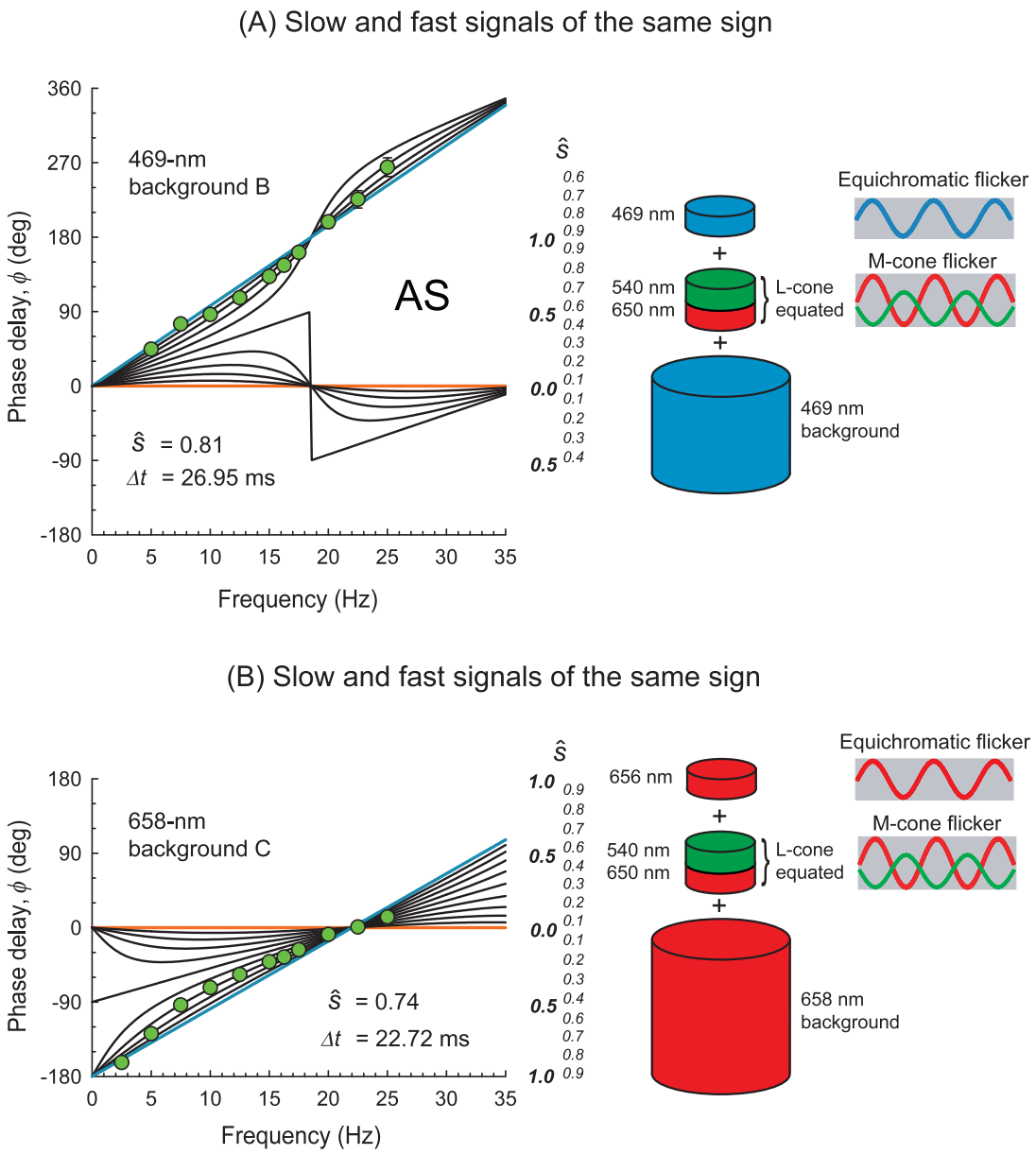

Figure 6. Panel (A) shows M-cone phase delays measured on a moderate background radiance, 469-nm background. The illustration on the right of panel (A) shows the stimuli: a 469-nm steady background on which is superimposed 469-nm "equichromatic" flicker and the L-cone equated counter-phase flickering 540-and 650-nm pair. The phase delays under this condition for AS (green symbols) are shown in the left graph with the best-fitting set of predictions for $+sM$ with values of $\hat{s} = 0.81$ and $\Delta t = 26.95$ ms. Panel (B) shows M-cone phase delays measured on a high background radiance, 658-nm background. The illustration on the right shows the stimuli: a 658-nm steady background on which is superimposed a 656-nm "equichromatic" flicker and an L-cone equated counter-phase flickering 540- and 650-nm pair that produce the M-cone flicker used to null the equichromatic flicker. The phase delays measured in this condition for AS (green symbols) are shown in the left graph with the best-fitting set of predictions for $-sM$ with values of $\hat{s} = 0.74$ and $\Delta t = 22.72$ ms.

simulated by the model can help to explain our data. In the graph in Panel (A) we show the characteristics for various values of $\hat{s}$ for slow and fast signals of the *same* sign separated by a Δt of 26.95 ms, and in the graph in Panel (B) we show the phase characteristics generated for values of $\hat{s}$ varying in 0.1 steps from 0 to 1 for slow and fast signals of the *opposite* sign separated by a Δt of 22.72 ms. From these comparisons, we can infer that the phase data in the Panel (A) are consistent with the M-cone signal's being the resultant of $+sM$ and $+fM$ components with $+sM > +fM$ (with the best-fitting weights for $\hat{s}$ and Δt of 0.81 and 26.95 ms, respectively). The data in Panel (B) are consistent with the M-cone signal's being the resultant of $-sM$ and $+fM$ compo-

Downloaded From: http://jov.arvojournals.org/pdfaccess.ashx?url=/data/journals/jov/936743/ on 02/20/2018

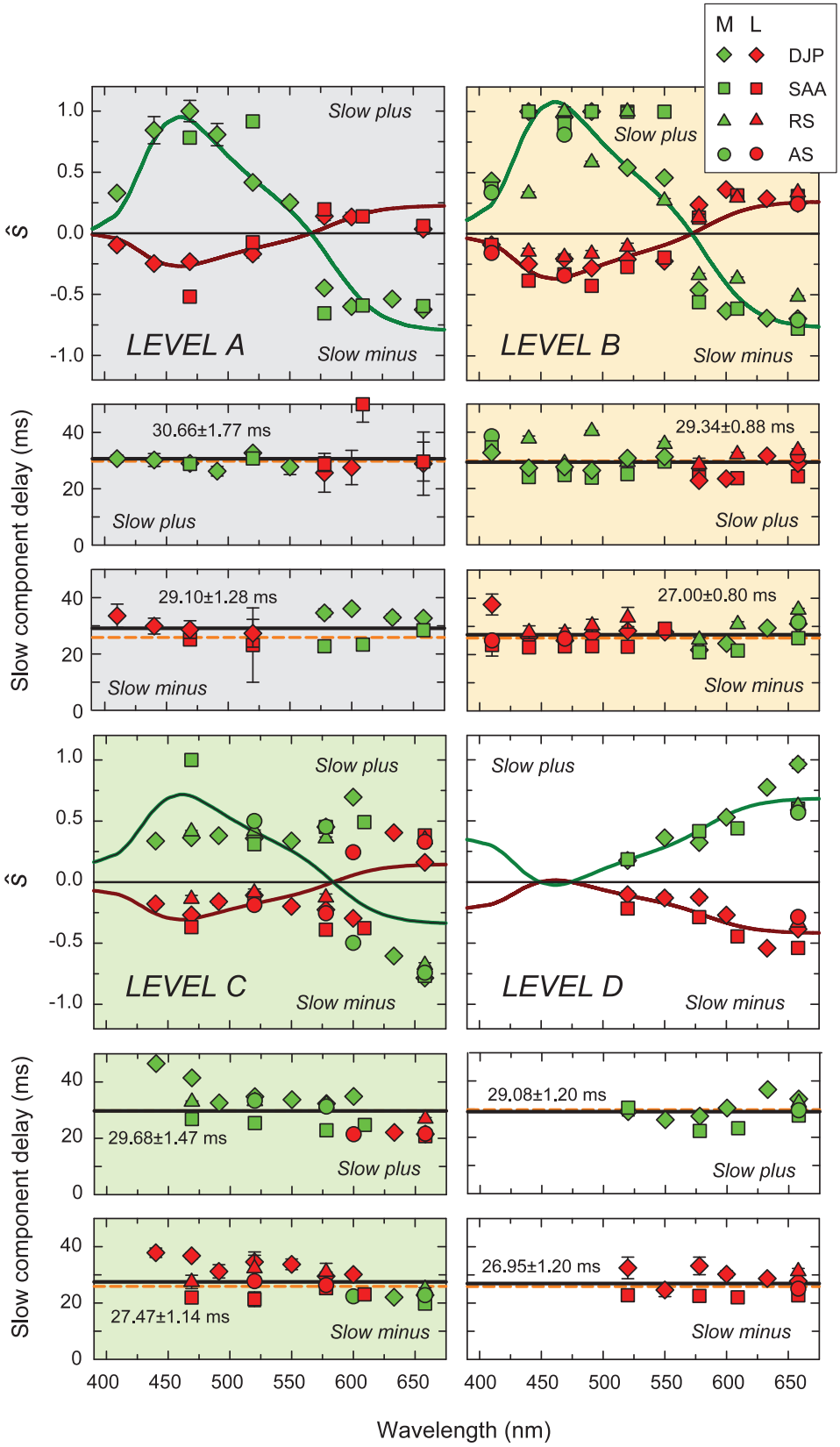

Figure 7. Each set of three graphs shows the best-fitting parameters with ±1 *SE* of the fitted parameter for the basic model (individually-fitted delays and slow signal weights) separately at the four different intensity levels. Data for DJP are plotted as diamonds, SAA as squares, RS as triangles, and AS as circles. The upper panel of each triplet shows $\hat{s}$ as a function of background →

Downloaded From: http://jov.arvojournals.org/pdfaccess.ashx?url=/data/journals/jov/936743/ on 02/20/2018

←

wavelength (nm); positive values correspond to $+s$ slow signals, negative values to $-s$ slow signals. The lower two panels show the delays (ms) of slow positive and slow negative signals also as a function of wavelength. Parameters for L-cone isolating stimuli are shown in red, those for M-cone isolating stimuli in green. The horizontal solid lines in the lower panels are the mean best-fitting delays averaged across observers and background wavelengths; the numbers in each panel are this mean and its standard error. The horizontal dashed, orange lines show the mean best-fitting delays averaged across observers if the time delay is fixed across background wavelength separately for the slow positive and slow negative signals (Model C). The smooth curves fitted to $\hat{s}$ in the upper panel of each set are discussed in the text.

nents with $|-sM| > +fM$ (the best-fitting weights for $\hat{s}$ and Δt were of 0.74 and 22.72 ms, respectively). The best-fitting values were derived from individual fits of the model defined by Equations 2 or 3 and 4 to each set of L- and M-cone data shown in each panel of Figures 1 through 4.

The model fits to each data set are shown in Figures 1 through 4 as black lines. Thirty-five different background wavelengths and radiances were used for DJP, 23 different for SAA, 13 different for RS, and 8 different for AS. A comparison of each set of L- and M-cone phase measurements with the predictions shows that each of them is consistent with one of the phase predictions. The fits were carried out using the standard nonlinear fitting Marquardt-Levenberg algorithm (Levenberg, 1944; Marquardt, 1963) implemented in SigmaPlot (Systat Software, San Jose, CA) or in MATLAB (MathWorks, Natick, MA). The best-fitting parameters are given in Table A5, A6, A7, and A8 in the Appendix for DJP, SAA, RS, and AS, respectively. We will consider the fits shown by the white lines in Figures 1 through 4 later.

Figure 7 plots the best-fitting parameters $\hat{s}$ and Δt for all the observers as a function of background wavelength (nm, linear axes). Each group of three graphs is plotted on a different background and shows data obtained at the different background levels indicated—A to D. To recap, the levels were A: Low levels (1.42–1.98 log Td), B: Moderate levels (2.64–3.09 log Td), C: High levels (3.83–4.33 log Td), and D: Very high or bleaching levels (5.13–5.40 log Td). The upper panel of each group of three shows the best-fitting $\hat{s}$ as a function of wavelength. The red symbols show the fits for L-cone isolating stimuli and the green symbols those for M-cone data. The best-fitting parameters for each observer are represented separately by the different symbols shown in the inset on the top right. The sign of $\hat{s}$ indicates whether the slow cone signal is positive or negative with respect to the fast cone signal. The curves fitted to the L- and M-cone parameters will be discussed subsequently.

The lower two panels show the best-fitting delays of the $+s$ and $-s$ signals, respectively. The minus and positive slow-signal delays have been plotted separately for the reasons discussed below. Red symbols again show best-fitting parameters for L-cone isolating stimuli, green symbols, for M-cones. The error bars are ± 1 standard error of the fitted parameter. The highly uncertain L-cone fitted parameters with very large standard errors for DJP (for levels 491A, 550A, and 633A) and for RS (for level 550B), are for conditions where the phase response is effectively flat at 0° and the model is simply fitting the noise, which are marked by asterisks in Tables A5 through A7, and are not plotted in Figure 7, nor are they used in fitting the model discussed below.

Several patterns can be seen in the fits and data for all four observers, and in the corresponding parameters plotted in Figure 7. For the shorter wavelength background and higher intensity longer wavelength background conditions, the form of the M-cone phase delays and model parameters suggest that the predominant M-cone signals are $+sM$ and $+fM$, whereas the form of the L-cone phase delays and the model parameters suggest that the predominant L-cone signals are $-sL$ and $+fL$. These conditions are highlighted by the gray panel colors in Figures 1 through 4. By contrast, for the lower intensity longer wavelength background conditions, the form of the M-cone phase delays and model parameters suggest that the predominant M-cone signals are instead $-sM$ and $+fM$, and the form of the L-cone phase delays, and the model parameters suggest that the predominant L-cone signals are $+sL$ and $+fL$. Those conditions are highlighted by the brown panel colors in Figures 1 through 4. Consequently, if a change in background wavelength or radiance is such that the panel background colors change from gray to brown or vice versa, then *both* the slow M- and the slow L-cone signals reverse in sign.

Three consistent features of the data and model are apparent in the original data shown in Figures 1 through 4 and in the dependence of $\hat{s}$ on background wavelength shown in the upper panels of the four quadrants of Figure 7. First, the slow L- and M-cone signals for a given set of conditions are invariably opposite in sign, so $-sM$ is found with $+sL$, and $+sM$ is found with $-sL$. The slow signals, in other words, are cone-opponent. Second, the values of $\hat{s}$ for M-cones are invariably greater than those for L-cones. Since $\hat{s}$ is a

Downloaded From: http://jov.arvojournals.org/pdfaccess.ashx?url=/data/journals/jov/936743/ on 02/20/2018

relative measure, this could mean either that $+fL > +fM$ or that $|-sM| > +sL$, and $+sM > |-sL|$. Given the finding that on average the L-cone contribution to the luminance pathway is about double the M-cone contribution (e.g., Cicerone & Nerger, 1989; Vimal, Smith, Pokorny, & Shevell, 1989; Carroll, Neitz, & Neitz, 2002; Hofer, Carroll, Neitz, Neitz, & Williams, 2005; Sharpe et al., 2011), it is plausible that $+fL > +fM$. However, given that there are also more L-cones than M-cones in the horizontal cell surrounds, it is also plausible that the slow M-cone weights are larger than the slow L-cone weights so that they balance in the surrounding network. Nonetheless, given the variability of numbers of M- and L-cones given in the papers just cited, there should be some observers in whom there are more M-cones than L-cones and in whom we would therefore expect the slow L-cone signals to dominate the phase measurements. We have not yet encountered such an observer. Third, the $\hat{s}$ values for the slow M- and L-cone signals vary systematically *together* with background wavelength, tending to be smaller near 550 nm but larger at longer and shorter wavelengths. We will return to this variation when we try to model it below.

In contrast to $\hat{s}$, Δt is remarkably constant across background wavelengths and radiances, as can be seen in the middle and lower panels at each background shown in Figure 7. The horizontal solid black lines indicate the mean values of Δt for the slow negative or positive M- and L-cone signals averaged across observers and background wavelengths, which along with ± 1 *SE*, are indicated in each panel. The differences between the slow positive and slow negative time delays are small, but are always in a consistent direction with the slow positive delays being greater by a few milliseconds than the slow negative delays.

The black lines in Figures 1 through 4 show the predictions of the basic model outlined in Figure 5 with simple time delays between fast and slow cone signals of different size and sign. The model's predictions are for individually fitted time delays between fast and slow cone signals of the same or opposite sign and, as can be seen, provide an excellent description of the phase measurements. The rows labelled A in Table 1 summarize how good these fits are for each observer in terms of the standard error of the regression (*SER*, in degrees) and the unadjusted and adjusted percentage coefficients of determination, R^2. [Note that for nonlinear regression, R^2 as a measure of goodness-of-fit is problematic (e.g., Kvalseth, 1985; Spiess & Neumeyer, 2010), so that as well as giving R^2 and adjusted R^2 values, we also give the standard errors of the regression (*SER*). These can be used to assess the precision of the predictions when the models have the same number of parameters, but there is no simple way of comparing the nonlinear models that are not nested.] The basic model does a good job of accounting for the data with adjusted R^2 values ranging from 90.9% to 96.5%, and *SER* values from 0.4° to 0.64°. The fits summarized in the rows labelled Models B to E of Table 1 are variations of the basic model, which will be discussed in the next section.

The upper three diagrams shown in Figure 8 are diagrammatic representations of the versions of the Basic model referred to as Models A to E in Table 1 and in the text. (The lower diagram shows an alternative model, which as described below, proved to be unsuccessful.)

Modifications to the basic model

We fitted a simplified time-delay model, referred to as Model B, on the basis that Δt is approximately independent of background wavelength and radiance (see Figure 7), and therefore fixed its value across conditions. The rows labelled Model B in Table 1 summarize the fits for a constant best-fitting delay for both the slow positive and slow negative signals. Compared to the fits of Model A in which Δt was allowed to vary, the adjusted R^2 percentages are worse, falling from between 90.9 and 96.5% to between 80.4 and 88.9% and *SER* values increasing from between 0.41° and 0.64° to between 0.69° and 1.23°. So although the differences in delay are small across conditions they are important.

For Model C, we allowed the Δt delays to take on different best-fitting constant values for the slow negative and slow positive signals. As would be expected from the individual fits, which suggested the positive slow signals were, on average, slightly slower than the negative slow signals, this improved the fits, but only slightly. The adjusted R^2 percentages fall to only between 83.6 and 89.2% and the *SER* values rose to between 0.63° and 1.09°, as summarized in the rows labelled Model C in Table 1. The general finding that Δt is consistently longer for the slow positive signals than for the slow negative ones by, in this case, 4.6, 2.0, 4.5, and 2.6 ms for DJP, SAA, RS, and AS, respectively. This is consistent with the results for the individually fitted Δt values (see Figure 7, and Tables A1 through A4) and is of potential importance in understanding the underlying causes of these effects. The fits for fixed Δt values for the slow and fast signal (without filtering) are plotted as white lines in Figures 1 through 4. (The mean Δt values across observers, ± 1 *SE*, which are 29.78 $\pm$ 1.76 ms for the slow positive signals and 25.85 $\pm$ 1.22 ms for the slow negative signals are plotted as dashed orange lines in the middle and lower panels of the four quadrants in Figure 7.) We consider the differences between these fits and the individually fitted delays below.

Downloaded From: http://jov.arvojournals.org/pdfaccess.ashx?url=/data/journals/jov/936743/ on 02/20/2018

Model	Observer	Corner frequency (Hz)	Δt (ms)	*SER* (degree)	R^2 (%)	Adjusted R^2 (%)
A	Δt and $\hat{s}$ individual-fitted to the M- and L-cone phase data for each condition (fits shown in Figures 1 through 4 as black lines)					
	DJP	X	Table A5	0.41	94.2	92.5
	SAA	X	Table A6	0.57	94.1	92.6
	RS	X	Table A7	0.64	92.6	90.9
	AS	X	Table A8	0.58	97.2	96.5
B	$\hat{s}$ individual-fitted to the M- and L-cone phase data for each condition with common delay					
	DJP	X	−30.5 ± 0.07	0.69	84.7	82.7
	SAA	X	−24.8 ± 0.07	0.75	90.1	88.9
	RS	X	−33.2 ± 0.08	1.00	82.3	80.4
	AS	X	−28.8 ± 0.13	1.23	87.9	86.5
C	$\hat{s}$ individual-fitted to the M- and L-cone phase data for each condition with common plus or minus delays (fits shown in Figures 1 through 4 as white lines)					
			Plus / *Minus*			
	DJP	X	−31.1 ± 0.07 / −26.5 ± 0.19	0.63	86.6	84.6
	SAA	X	−25.0 ± 0.08 / −23.0 ± 0.19	0.72	90.5	89.3
	RS	X	−33.3 ± 0.11 / −28.8 ± 0.34	0.94	84.3	83.6
	AS	X	−29.7 ± 0.12 / −25.1 ± 0.28	1.09	90.4	89.2
D	Δt and $\hat{s}$ individual-fitted to the M- and L-cone phase data for each condition with common low-pass filter					
	DJP	7.6 ± 0.16	Not tabulated	0.28	97.4	96.6
	SAA	11.4 ± 0.42	Not tabulated	0.49	95.8	94.7
	RS	13.0 ± 0.69	Not tabulated	0.60	93.5	92.0
	AS	12.0 ± 0.41	Not tabulated	0.45	98.4	98.0
E	$\hat{s}$ individual-fitted to the M- and L-cone phase data for each condition with common delay and a common low-pass filter					
	DJP	6.6 ± 0.24	−19.0 ± 0.14	0.55	90.3	89.0
	SAA	10.1 ± 0.44	−15.8 ± 0.16	0.66	92.4	91.5
	RS	8.0 ± 0.44	−21.8 ± 0.27	0.82	88.0	86.6
	AS	10.0 ± 0.70	−19.1 ± 0.31	1.04	91.1	89.9

Table 1. Model variations, summary of fits. *Note*: Best-fitting parameters and ±standard error of the fitted parameter, standard error of the residuals (degrees), unadjusted and adjusted R^2.

For Models D and E, we attempted slightly more complicated models. The assumption of a simple time delay between the slow and fast signals implies that $\hat{s}$ is independent of temporal frequency, and consequently that there is no dependence on frequency in the strength of the slow signal relative to the strength of the fast. However, signals are usually subject to relative high-frequency loss in visual processing streams (e.g., Van De Grind, Grüsser, & Lunkenheimer, 1973). We simulated this loss by adding a low-pass filter to the slow signals in series with the delay (see Figure 8) with an amplitude response (A_s) given by:

$$A_s = \left[1 + (v/v_c)^2\right]^{-\frac{1}{2}}, \quad (5)$$

where v is frequency and v_c is the filter's corner frequency both in Hz. The phase delay of the filter (θ_s) is

$$\theta_s = \arctan(v/v_c). \quad (6)$$

In this modification to the model, A_s multiplies s, the magnitude of the slow signal, thus affecting s/f in Equation 3, while θ_s adds to the phase difference $\Delta\theta$, thus affecting Equations 2 through 4. The corner frequency was assumed to be fixed across conditions.

Downloaded From: http://jov.arvojournals.org/pdfaccess.ashx?url=/data/journals/jov/936743/ on 02/20/2018

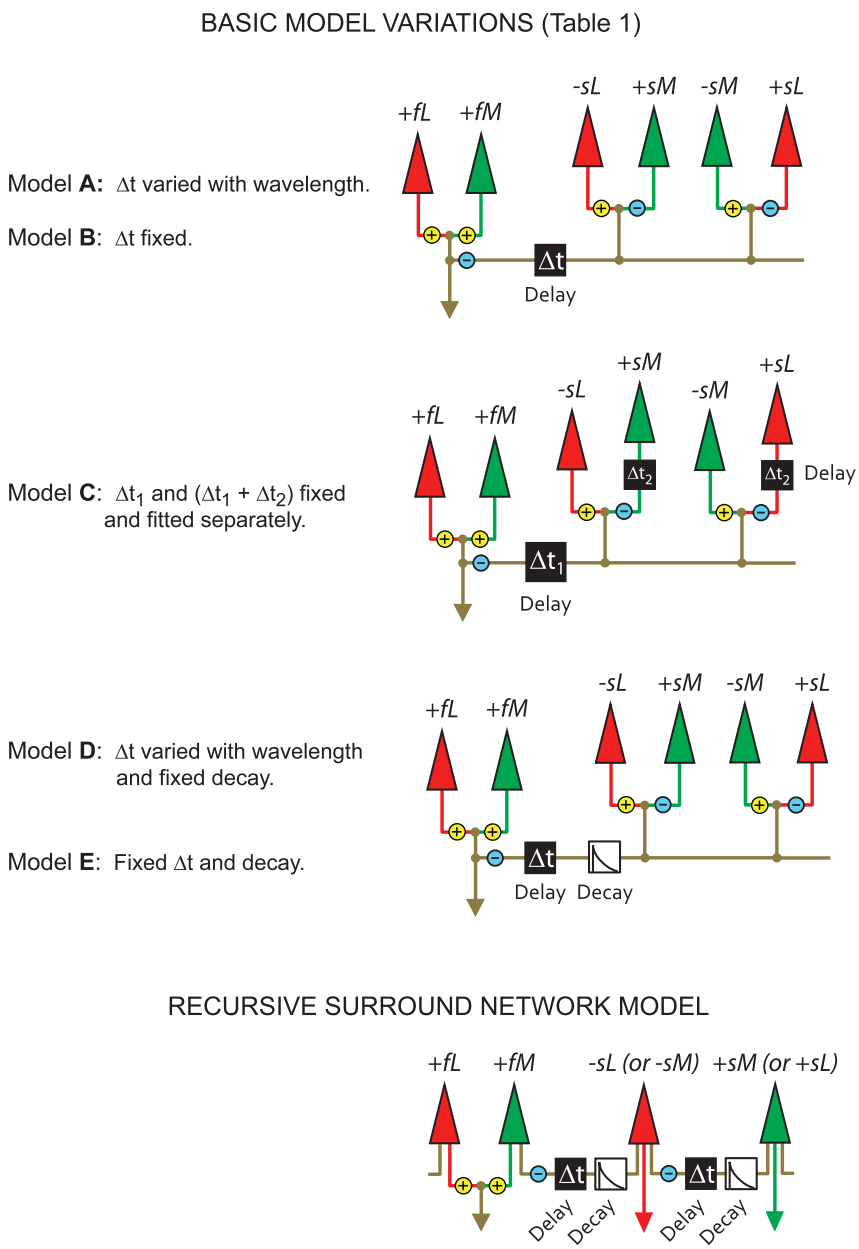

Figure 8. The upper three diagrams show schematic representations of variations of the basic model, which we refer to as Models A to E (see Table 1). The lower diagram is a schematic representation that shows an alternative model referred to as the recursive network surround model. In all diagrams, the red and green triangles represent L- and M-cones, respectively. The model connections are shown by continuous lines, and can be excitatory, as indicated by the plus symbols on yellow circles, or inhibitory, as indicated by the minus symbols on blue circles. Significant time delays in the connections are denoted by "Δt" within black boxes. Low pass filtering stages are denoted by exponential decays within white squares. $+fL$ and $+fM$ indicate the fast cone inputs to the luminance channel (the output of which is shown by the brown arrows), while $+sL$, $+sM$, $-sL$, and $-sM$ indicate the slow inputs ("slower" because of delays and/or low pass filtering). Models A and B have a delay of Δt between the slow and fast signals. Model C has a delay of Δt_1 between the slow and fast signals with an extra delay of Δt_2 added to the $+sM$ and $+sL$ signals. Models D and E have a delay of Δt and a low-pass filter between the slow and fast signals. In the recursive inhibitory surround network model (bottom diagram), $-sL$ and $-sM$ are subjected to one stage of low-pass filtering and delay, while $+sM$ and $+sL$ are subjected to two stages.

The rows labelled Model D in Table 1 summarize the fits. Because the low-pass filter introduces delays, the addition of a low-pass filter with best-fitting corner frequencies between 10.8 and 21.4 Hz for the four observers reduces the required time delays by about 10 ms (not tabulated), and improves the adjusted R^2 values very slightly from between 90.9% and 96.5% to between 91.4% and 97.4%, and reduces the *SER* from between 0.41° and 0.64° to between 0.33° and 0.62°. The values of $\hat{s}$ (also not tabulated) did not change

Downloaded From: http://jov.arvojournals.org/pdfaccess.ashx?url=/data/journals/jov/936743/ on 02/20/2018

significantly. From this, we can conclude that a low-pass filter added to the slow signals is *consistent* with the phase delay measurements, but not necessary to account for them. We also carried out fits in which the corner frequency, like $\hat{s}$, was allowed to vary across conditions. While this resulted in higher adjusted R^2 percentages of between 94.1% and 98.0%, the increases were modest, and there were several clear cases of overfitting, where ν_c took on implausible values to account for relatively small deviations from the basic model.

Finally, the rows labelled Model E in Table 1 summarize a model fit in which a constant Δt and a constant low-pass corner frequency were assumed. The best-fitting time delays were between 15.8 and 21.0 ms and the corner frequencies of the low-pass filter between 6.6 and 10.1 Hz. Compared to the Model **A** fits the adjusted R^2 percentages fell from between 90.9% and 96.5% to between 86.6% and 91.5% and the *SER* values rose from between 0.41° and 0.64° to between 0.55° and 1.04°. Again these fits show that the slowness of the slower signals is consistent with a delay and a low-pass filter.

General discussion

Although the results shown in Figures 1 through 4 appear complex, we have demonstrated that they can be accounted for by a relatively simple model in which the representations of L- and M-cone flicker are comprised of not only a fast copy of the flicker signal, but also a slow copy that is delayed by roughly 30 ms and varies in strength and sign with both background wavelength and radiance. Modifications to the model suggest that in addition to a delay some filtering is involved, and that the $+sM$ and $+sL$ signals might be slightly more delayed (or filtered) than the $-sM$ and $-sL$ signals. In the next sections, we place our work in the context of other psychophysical and physiological data and models, and develop what we believe to be a physiologically plausible working model that is consistent with our results.

Phase delays and selective cone adaptation

The phase delays for flickering M- or L-cone isolating lights were measured and defined relative to the "equichromatic" target, which we assume generates mainly fast $+fL$ and $+fM$ signals. This is undoubtedly an approximation, since the pair of targets used to produce cone-isolating flicker, which are superimposed on the equichromatic target and background, will slightly change the chromaticity away from that of the background wavelength in the region of the target. Yet, in terms of the model, the approximation is good enough to yield data that are consistent with a time delay between the slow and fast signals.

There is, however, one important factor that our basic model ignores. Given that light adaptation speeds up the cone response (e.g., Rogers & Anstis, 1972; Campbell, Rothwell, & Perry, 1987; Stockman, Langendörfer, et al., 2006), selective L- or M-cone adaptation will introduce phase delays between the $+fM$ and $+fL$ signals. On middle-wavelength backgrounds, the phase delays will be relative small, since the M- and L-cones have similar spectral sensitivities at middle-wavelengths, but on long- and short-wavelength backgrounds, where the L- and M-cone spectral sensitivities are different, the phase delays between the $+fM$ and $+fL$ flicker signals may become significant (the delays can be estimated from data in Stockman, Langendörfer, et al., 2006). For example, in quantal units, the M-cones are 1.7 times more sensitive to our 469-nm background than the L-cones, whereas the L-cones are 7.24 and 12.60 times more sensitive than the M-cones to the 633 and 658-nm backgrounds, respectively (Stockman & Sharpe, 2000). Thus, we would expect $+fL$ to be phase delayed on short-wavelength backgrounds and $+fM$ to be phase delayed on long-wavelength backgrounds.

By individually fitting the time delays to the phase delay data for each background condition, the fit can compensate for the effects of selective adaptation between the M- and L-cones by small adjustments in Δt, since the phase delays or advances produced by selective adaptation can be approximated—at least at low temporal frequencies—by small adjustments in time delay (see Stockman, Langendörfer, et al., 2006). We can assess the extent of those adjustments by comparing the individually fitted time delays (Model A, black lines in Figures 1 through 4) with fits in which the time delay was held constant separately for the slow minus and the slow plus signals across background conditions (Model C, white lines in Figures 1 through 4).

Given the assumption that fast signals are dominated by L-cone signals (see above), the effect of selective adaptation should be most apparent in the M-cone data. On short-wavelength backgrounds, the fits with constant Δt should overestimate the M-cone phase delays since the M-cones are more adapted than the L-cones (i.e., the fits shown by the white lines should be steeper—slower—than those shown by the black lines.) By contrast, on long-wavelength backgrounds the fit with constant Δt should underestimate the M-cone phase delays since the M-cones are less adapted than the L-cones (i.e., the fits shown by the white lines should be shallower—faster—than those shown by the black lines.)

Downloaded From: http://jov.arvojournals.org/pdfaccess.ashx?url=/data/journals/jov/936743/ on 02/20/2018

The pattern of results and fits shown in Figures 1 through 4 generally follow this pattern, but the differences in the time delays that were found, and which we assume to be due to selective chromatic adaptation, were relatively small compared to time delays between the slow and the fast signals.

Previous psychophysical evidence for slow cone inputs

The data of Lindsey et al. (1986), and Swanson et al. (1987), were the first indirect, potential evidence for sluggish, negative cone inputs to the luminance channel, but were not originally interpreted as such. Direct evidence for this input was obtained, using M-cone isolating stimuli, by Stockman and Plummer (1994), who found a $-sM$ signal delayed by approximately 25 ms and inverted relative to the $+fL$ signal (a delay that was subsequently confirmed by Stromeyer et al., 1997).

Evidence for a slow signal of the same sign as the $+fM$ and $+fL$ signals was obtained by Stockman, Montag, et al. (1991) and Stockman et al. (2005), who observed a $+sM$ signal on an intense red field. This signal was in phase with the $+fM$ and $+fL$ signals at low frequencies, but in opposite phase near 16 Hz, where the $+fM$ and $+sM$ signals destructively interfere (and reduce M- cone sensitivity). A similar $+sM$ signal has been observed on green and blue backgrounds (Stromeyer et al., 1997), a finding which we confirm in this work. Stromeyer et al. (1997) inferred the presence of the spectrally opponent $+sM-sL$ and $-sM+sL$ signals from phase data obtained mainly from motion, but also from flicker experiments made on backgrounds between 500 nm and 650 nm. Importantly, they identified the change from $+sM-sL$ to $-sM+sL$ with increasing background wavelength, results which were confirmed by Stromeyer et al. (2000). They did not recognize the link between their work and our earlier work identifying the $+sM$ and $-sM$ signals, although that work had only been published in abstract form (Stockman, Montag, et al., 1991; Stockman & Plummer, 1994). Their novel contribution was to observe that $+sM-sL$ signals predominate on shorter wavelength fields. The idea that sluggish "chromatic" $-sM+sL$ signals interact with faster "luminance" signals on longer wavelength fields was proposed several years earlier by Smith et al. (1992) to account for data obtained from macaque magnocellular-projecting (MC) ganglion cells. They assumed that the $+fM+fL$ signals are the center response of the ganglion cell, while the $-sM+sL$ signals are the surround response. A reduction of the $+sM-sL$ and $-sM+sL$ signals, relative to the $+fM+fL$ signals occurs with decreasing spatial frequency, which suggests a spatially opponent surround (Kremers, Yeh, & Lee, 1993; Stromeyer et al., 1997).

In 2005, we reported slow $-sM+sL$ signals on low to moderate intensity 658 nm, red fields (Stockman & Plummer, 2005b), slow $+sM-sL$ signals of opposite sign on high intensity red fields (Stockman et al., 2005); and a rapid transition between them in the intervening intensity range (Stockman & Plummer, 2005a). We proposed that these changes reflect the coexistence of multiple cone inputs to the luminance pathway, the relative strengths of which depend on chromatic adaptation. In particular, since $+sL-sM$ and $-sL+sM$ are in opposite phase, and therefore destructively interfere; only the stronger affects the measured phase delay of the cone flicker signal. Here, we determined how these signals depend on chromatic adaptation.

We assume that the achromatic channel subserving flicker perception has in addition a slow $-sS$ input, the evidence for which comes from other work (Stockman et al., 1987; Lee & Stromeyer, 1989; Stockman, MacLeod, et al., 1991). See Figure 6 of Stockman & Plummer (2005a).

Physiological evidence for slow cone inputs

A crucial question is where the slow signals arise in the visual system. As we describe in this section, some of the characteristics of the slow cone signals can be identified in recordings from primate horizontal cells and from magnocellular ganglion cells.

Horizontal cells

There are two classes of horizontal cells in primate retina, the H1 cells, which contact almost exclusively L- and M-cones, and the H2 cells, which preferentially contact S-cones but also contact L- and M-cones (Ahnelt & Kolb, 1994; Dacey, Lee, Stafford, Pokorny, & Smith, 1996; Goodchild, Chan, & Grünert, 1996). Through inhibitory feedback to cones, the horizontal cells provide the spatially opponent inhibitory surrounds for cones (Baylor, Fuortes, & O'Bryan, 1971) and for bipolar cells (Werblin & Dowling, 1969), although the bipolar cell surround may also be formed through direct inhibitory feedforward connections (see Thoreson & Mangel, 2012). In primates and man, all cone contacts to horizontal cells have the same sign, so that the horizontal cells are not inherently color opponent (Boycott, Hopkins, & Sperling, 1987; Dacheux & Raviola, 1990; Dacey et al., 1996).

Compelling evidence for the delay in physiological recordings can be found in horizontal H1 data measured by Smith, Pokorny, Lee, and Dacey (2001) to investigate sensitivity regulation in the outer retina. Data from their figures 4A and 7A have been replotted

Downloaded From: http://jov.arvojournals.org/pdfaccess.ashx?url=/data/journals/jov/936743/ on 02/20/2018

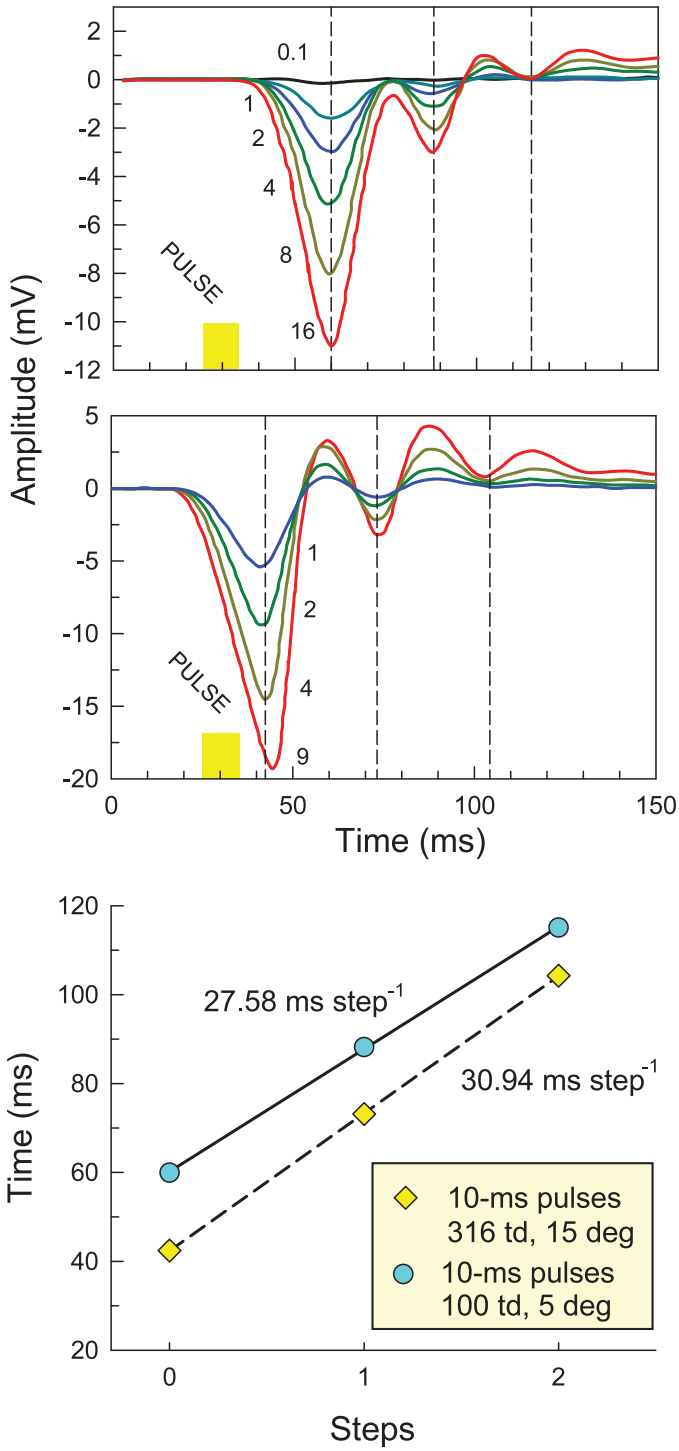

Figure 9. Horizontal cell recordings from Smith et al. (2001). The upper panel reproduces data from their figure 4A and shows responses to 5° diameter, 10-ms luminance increments with contrasts 0.1, 1, 2, 4, 8, and 16, plotted with differently colored solid lines, all obtained on a 2 $\log_{10}$ photopic Td background. The middle panel reproduces data from their figure 7A, and shows response obtained on a 2.5 $\log_{10}$ Td background to 15° diameter, 10-ms contrast increments with contrasts of 1, 2, 4, and 16 again plotted in differently colored lines—amplitude (mV) is plotted against time (ms). The vertical dashed lines in the upper and lower panels show the mean of the greatest responses (which are negative-going) across contrasts. The means from the upper (blue circles) and middle (yellow diamonds) panels are plotted in the lower panel as a function of "steps," which number the successive peaks and troughs. The means in the lower panel have been fitted with regression lines (solid lines), which have best-fitting slopes of 27.58 ms per step (blue circles) and 30.94 ms per step (yellow diamonds). The flash onset (shown as a yellow rectangle in our Figure 9) may be wrong in their figure 7A.

in the upper and middle panels of Figure 9, respectively. The recordings replotted in the upper panel were obtained on 2 $\log_{10}$ photopic Td backgrounds using 5° diameter, 10-ms luminance increments with contrasts of 0.1, 1, 2, 4, 8, and 16; those replotted in the middle panel were obtained at 2.5 $\log_{10}$ Td using 15° diameter, 10-ms contrast increments with contrasts of 1, 2, 4, and 16. Different colored lines show the response to increments of different contrast. The ordinate shows intracellular voltage as a function of time with the time of occurrence and duration of the 10-ms stimulus increment indicated by the yellow rectangle.

As noted by the authors, the recordings show oscillations that decrease in amplitude over time but align across different pulse contrasts. To quantify the timing of the oscillations, we have averaged the location of the troughs in each panel across contrasts. The means are indicated by the vertical dashed lines and are plotted in the lower panel as blue circles and yellow diamonds for the means in the upper and middle panels, respectively. A regression line has been fitted to each set of means and has a delay per oscillation of 27.58 ms (solid line, blue circles, $R^2 = 1.00$) and 30.94 ms (dashed line, yellow diamonds, $R^2 = 1.00$). If sinusoidal signals are used rather than brief, single flashes, a model with a delay of 29.26 ms (the mean of the two regression fits) predicts that the copies of the sinusoidal signals will all be in phase near 34 Hz, and indeed for larger stimulus diameters there is clear evidence in figures 2 and 3 of Smith et al. (2001) for a resonance shoulder or peak in the horizontal-cell amplitude-sensitivity data for flicker near 34 Hz. Note, however, the resonance will be reduced by the slow minus signal that, according to our model, will destructively interfere.

The delay of nearly 30 ms is too long to be the feedback mediated by single horizontal cells, which would be expected to be comparable to the center-surround delay of parvocellular ganglion cells. Those delays are typically found to be between about 2 and 9 ms (Lee, Martin, & Valberg, 1989a; Smith et al., 1992; Lee, Pokorny, Smith, & Kremers, 1994; Benardete & Kaplan, 1997), although delays as long as 16 ms or more have been reported (Gouras & Zrenner, 1979; Gielen, van Gisbergen, & Vendrik, 1982). However, the spatial

Downloaded From: http://jov.arvojournals.org/pdfaccess.ashx?url=/data/journals/jov/936743/ on 02/20/2018

extent of the horizontal cell net-work derives from two sources: a small, localized surround that is delimited by horizontal-cell dendritic trees, which receive strong direct cone inputs, and a larger, extended surround, which depends on weaker synergistic inputs across gap junctions between horizontal cells (Packer & Dacey, 2002, 2005). In the fovea, the localized horizontal-cell surrounds are relatively small and comparable in spatial extent to foveal midget cell surrounds (Packer & Dacey, 2002). The synergistic horizontal-cell-network surround feeding back onto cones may be the origin of the slow cone signals that we observe.

Magnocellular ganglion cells

At the next stage of neural processing, a mixture of L- and M-cones jointly contact ON and OFF diffuse bipolar cells, which in turn contact ON and OFF parasol ganglion cells of the same polarity (e.g., Polyak, 1941; Boycott & Dowling, 1969; Mariani, 1981; Boycott & Wässle, 1991; Jacoby, Stafford, Kouyama, & Marshak, 1996; Jacoby, Wiechmann, Amara, Leighton, & Marshak, 2000). In the fovea, diffuse bipolar cells contact about five to 10 L- and M-cones through the bipolar cells' dendritic arborisations (Boycott & Wässle, 1991; Calkins, Tsukamato, & Sterling, 1996; Calkins & Sterling, 2007), so that the spectral sensitivities of diffuse bipolar centers will be a combination of the L- and M-cone spectral sensitivities. The diffuse bipolar cells and parasol ganglion cells form the substrate of the magnocellular pathway that projects to the cortex via the magnocellular layers of the LGN (Leventhal, Rodieck, & Dreher, 1981; Perry, Oehler, & Cowey, 1984; Rodieck, Binmoeller, & Dineen, 1985). The magnocellular pathway is thought to provide the physiological substrate of the psychophysical luminance or achromatic pathway (e.g., Livingstone & Hubel, 1987; Lee, Martin, & Valberg, 1988; Lee, Pokorny, Smith, Martin, & Valberg, 1990; Smith et al., 1992), and thus to be responsible for psychophysical performance in our achromatic flicker cancellation task.

Given the clear evidence for the slow, or delayed, signals in horizontal cell recordings, a comparable signal should be found in magnocellular ganglion cell recording. And, indeed, many of the characteristics of the slow signals that we identify psychophysically can be at least tentatively identified in the physiological recording of primate magnocellular ganglion cells of Lee and his colleagues, which we describe next. In making these comparisons it is important to note that many of the physiological measurements (e.g., Lee et al., 1990; Smith et al., 1992; Yeh, Lee, & Kremers, 1995; Lee & Sun, 2009), with one notable exception in which backgrounds were used (Lee & Sun, 2004), were carried out under a set of experimental conditions that were constrained by the use of a pair of 638- and 554-nm LEDs, the intensities of which were adjusted to be of approximately equal luminance and used to produce the modulated temporal waveforms driving the cells. Together, the pair produced a time-averaged chromaticity approximately equal to a light of 595 nm (see p. 2224 of Lee et al., 1990). This stimulus was varied in mean luminance from low levels up to about 3.5 $\log_{10}$ photopic Td. In terms of our experimental conditions, the physiological conditions correspond most closely to the 600C or 609C conditions used for DJP, SAA and RS and to the 600D or 609D conditions for DJP and SAA (see Figures 1 through 3). In addition to the fast signals, the predominant slow signals we found under these conditions were the $-sM$ and $+sL$ signals. Consequently, the $+sM$ and $-sL$ signals would not be expected to be prominent in magnocellular data obtained using the conditions used in the physiological experiments.

Smith et al. (1992) used the 638-nm (red) and 554-nm (green) LEDs (set at 3.3 $\log_{10}$ Td and using a 4.7° diameter target) to measure the effect of varying the phase of sinusoidal modulations of the red and green LEDs on the magnocellular ganglion cell response. As expected, their results are consistent with the psychophysical results obtained under our 600C and 609C conditions. In particular, at low frequencies, the phase differences in Smith et al.'s data between the red and green lights show an increasing phase advance of the red LED relative to the green LED with decreasing frequency (their figure 7). That phase advance is consistent with the green modulation's generating primarily the $-sM$ signal seen in our data. Little evidence for other signals can be seen under these physiological measurements. By using red and green modulations rather than L- and M-cone-isolating stimuli, some of the detail seen in our data is lost because the cone signals are mixed (see, for example, Stockman & Plummer, 2005b). We next consider some important variations to the basic physiological experimental conditions with the 638- and 554-nm LEDs.

In one important experiment, Yeh et al. (1995) used the 638 and 554-nm LEDs to generate M- and L-cone-isolating modulations to measure magnocellular ganglion cell responses. We have replotted the data from panels A through C of their figure 6 in our Figure 10, which shows the response of an OFF-center magnocellular retinal cell (impulses s^{-1}) as a function of cone contrast (%) of a 9.8 Hz sinusoidal stimulus. Their measurements were made at a mean intensity of 2.3 $\log_{10}$ Td using either L-cone-isolating stimuli (red symbols), M-cone-isolating stimuli (green symbols) or luminance stimuli (yellow symbols). The upper panel of Figure 10 shows the 1st harmonic of the response as a function of cone contrast and the lower panel, the 2nd

Downloaded From: http://jov.arvojournals.org/pdfaccess.ashx?url=/data/journals/jov/936743/ on 02/20/2018

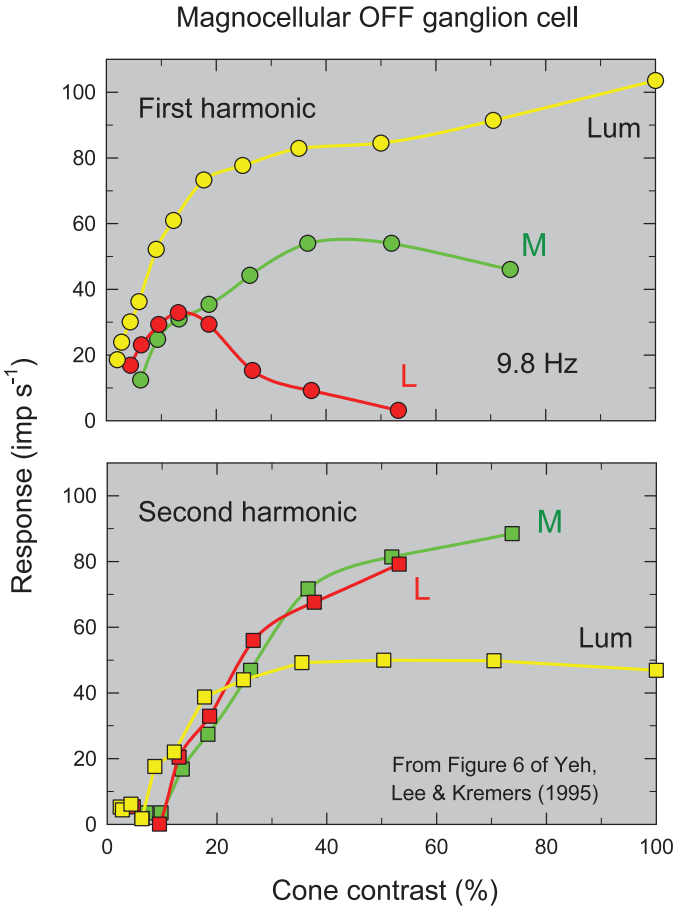

Figure 10. Responses of an OFF magnocellular ganglion cell reproduced from panels A through C of figure 6 of Yeh, Lee, and Kremers (1995) who used 638 and 554-nm LEDs to generate M- and L-cone-isolating and luminance modulations at 2.3 $\log_{10}$ Td. First harmonic (upper panel) and second harmonic (lower panel) cell responses (in impulses per second) to a 9.8-Hz sinusoidal stimulus are plotted as a function of cone contrast (%) for L-cone-isolating modulation (red symbols and lines), M-cone-isolating modulation (green symbols and lines) and luminance modulation (yellow symbols and lines).

harmonic of the response also as a function of cone contrast. (The sinusoidal stimuli contained only the 1st harmonic so that the 2nd harmonic is a distortion product generated by nonlinearities in the visual system.) The authors concluded that the results "showed more complex properties indicative of post-receptoral processing" (their abstract). In fact, the complex properties are broadly consistent with our model, and the expectation that under these conditions the predominant signals are $+sL$ and $-sM$ and $+fL$ and $+fM$. The differences between the first harmonic L- and M-cone responses are consistent with the slow +L and fast +L signals cancelling each other at intermediate frequencies as the cone contrast grows (Stockman & Plummer, 2005b; Stockman et al., 2005). By contrast, the $-sM$ and $+fM$ signals do not cancel each other to the same extent because they become more in phase at intermediate frequencies (see above). The luminance responses shown in Figure 10 (yellow symbols) are also consistent with the "equichromatic" reference modulations used in our experiments, which, we assume, generate small slow signals. These conclusions are bolstered by M- and L-cone-isolating measurements made by Lee & Sun (2009) fourteen years later. In figure 8 of that paper, they show the responses of an ON magnocellular ganglion cell to L- and M-cone-isolating stimuli at 2.4 and 9.8 Hz. The responses reveal marked frequency-doubled (2nd harmonic) responses consistent with the M- and L-cone slow and fast first harmonic signals partially cancelling each other but leaving an uncancelled 2nd harmonic component—perhaps the result of half-wave rectification after the horizontal cell network (see also below).

In another revealing experiment, Lee and Sun (2004) measured the effect of varying the phase of 638- (red) and 554-nm (green) LEDs on the response of magnocellular ganglion cells but with three different additional 3 $\log_{10}$ photopic td chromatic backgrounds at 470, 554, and 638 nm. The results on the 638-nm background were comparable to those of Smith et al. (1992) in showing that the response to the 638-nm modulation leads the response to the 554-nm modulation, which is consistent with the predominance of the $-sM$ signal under those conditions (see Figures 1 through 4). Their results on the 470-nm background, however, showed instead that the response to the 554-nm modulation leads that of the 638-nm modulation. This reversal is, of course, consistent with our short-wavelength background measurements and the predominance of the slow $+sM$ signal under those conditions (see Figures 1 through 4).

Finally, in a complex series of experiments, Lee and Sun (2009) investigated the "chromatic input" to magnocellular cells by modulating the 658- and 554-nm LEDs at 3.3 $\log_{10}$ Td to produce chromatic and luminance modulations, and, in some experiments, they used M- and L-cone-isolating modulations. An important aspect of their work concerned the frequency-doubled or second harmonic response of magnocellular ganglion cells that persists when the M- and L-cones are modulated in opposite phase at equiluminance so cancelling the first harmonic (Gouras & Eggers, 1983; Schiller & Colby, 1983; Lee, Martin, & Valberg, 1989b). Importantly, the second harmonic decreases as the target size is decreased, and is much weakened if only an annulus around the center is modulated (Lee et al., 1989b). Lee and Sun (2009) confirmed these results and found in their modelling of the responses that the radius of the retinal extent over which the "chromatic" second harmonic response was found was 19.3 ± 6.9 min. That radius was (a) larger than the 12.4 ± 5.1-min radius of magnocellular ganglion cell center, but (b)

Downloaded From: http://jov.arvojournals.org/pdfaccess.ashx?url=/data/journals/jov/936743/ on 02/20/2018

smaller than the 56.8 ± 29.2-min radius of the magnocellular surround, and (c) similar to the surround radius of parvocellular ganglion cells. From this, they concluded that the second harmonic was a parvocellular input to the magnocellular pathway that was "mediated through, for example, a small-field amacrine cell" (p. 15). Moreover, rather than attributing the second harmonic to an arbitrary nonlinear distortion as in previous work (Lee et al., 1989b), Lee and Sun (2009) provide evidence that the second harmonic is linked to half-wave rectification.

Several of the effects found by Lee and Sun (2009) can be related to the model we propose. The frequency-doubled (second harmonic) responses and the attenuated first harmonic responses found using M- and L-cone isolating flicker and chromatic flicker, as Lee and Sun (2009) show in their figure 8, are consistent with flicker interactions and cancellations between the slow and fast M- and L-cone signals. Moreover, the "chromatic" parvocellular response may correspond to responses of single cones and their surrounds feeding back into the network. The nonlinearity that produces the second harmonic is likely to correspond to the half-wave rectification and partition of the photoreceptor signal into ON and OFF pathways that also occurs in the outer retina (see also Stockman, Henning, & Rider, 2017).

In conclusion, the signatures of the slow cone signal are evident in both horizontal cell and magnocellular ganglion recordings pointing to a retinal origin for the slow signals probably in the extended horizontal cell surround.

Recursive network surround model

An alternative model that we explored in considerable detail (and described in abstract form in Stockman, 2013) was a recursive surround network model, in which the slow signals were assumed to be the overall or resultant responses of a recursive network of discrete components linked by inhibitory connections. Each step in the network was assumed to add a delay (with or without low-pass filtering), and at each step there was a change in the sign of the signal. We assumed that the slow positive signals were the result of even steps through the network dominating the slow signal (2-steps, 4-steps, and so on), whereas the slow minus signals were the result of odd steps dominating the slow signal (1-step, 3-steps, and so on). Thus, the step delay is approximately half the delay of the basic model. The lower diagram in Figure 8, above, showed a schematic of 1- and 2-steps of this model. Although we had some initial success in fitting this model to the phase delay measurements shown in Figures 1 through 4, we found that the fits typically converged onto model forms that were consistent with the basic model described above. For example, the slow positive signals tended to be accounted for by signals that were combinations of mainly 2-steps and 1-step in fixed ratio, whereas the slow negative ones tended to accounted for by signals that were combinations of mainly 3-steps and 2-steps in fixed ratio. These fixed ratios simply produced approximately the *same* positive and negative delays, as required by the time-delay model, rather than having a plausible or interpretable mechanistic role.

A working model

In this section, we develop a working model to account for the variations in $\hat{s}$ with background wavelength (λ). We will refer to these functions as $\hat{s}_M(\lambda)$ and $\hat{s}_L(\lambda)$ for the M- and L-cones, respectively. The various modifications to the basic fit, described above and summarized in Table 1, produced $\hat{s}_M(\lambda)$ and $\hat{s}_L(\lambda)$ values that were comparable to those obtained with fits of basic model plotted in Figure 7 and tabulated in Tables A5 through A8. Here, we focus on the values produced by the basic model.

As seen in Figure 7, $\hat{s}_M(\lambda)$ is generally larger than $\hat{s}_L(\lambda)$ by a roughly constant factor, and the two are of opposite sign. At the lower intensity levels, A and B, the functions reach a maximum for $\hat{s}_M(\lambda)$ and a minimum for $\hat{s}_L(\lambda)$ at 469 nm, change sign between 550 and 578 nm, and then decrease in the case of $\hat{s}_M(\lambda)$, or increase in the case of $\hat{s}_L(\lambda)$, with further increases in wavelength. Empirically, the shapes of the functions at levels A and B are similar to the shapes of cone-opponent functions of the form $M(\lambda)/L(\lambda)$, such that $\hat{s}_M(\lambda)$ and $\hat{s}_L(\lambda)$ can be approximated by

$$\hat{s}_M(\lambda) = a_M\left[\frac{M(\lambda)}{L(\lambda)} - k\right] \text{and } \hat{s}_L(\lambda) = a_L\left[\frac{M(\lambda)}{L(\lambda)} - k\right], \quad (7)$$

where $M(\lambda)$ and $L(\lambda)$ are the Stockman and Sharpe (2000) 2° cone fundamentals, a_M and a_L are slow M and L-cone weights, respectively, and k is an additional constant in to both of the L- and M- functions. The value of k determines where the sign of the slow signal changes from positive to negative.

The model represented by Equation 7 has been fitted to $\hat{s}_M(\lambda)$ and $\hat{s}_L(\lambda)$ at each of the four levels. In the upper panels of each of the four quadrants of Figure 7, the M- and L-cone fits are shown by the green and red solid lines, respectively. The best-fitting parameters with ±1 *SE* of the fitted parameter and the adjusted R^2 percentages are given in Table 2.

The fits at Levels A, B, and D are plausibly good with adjusted R^2 of between about 85% and 94%, but the fit for Level C is much poorer. The poorer fit for Level C probably reflects the transition from functions

Downloaded From: http://jov.arvojournals.org/pdfaccess.ashx?url=/data/journals/jov/936743/ on 02/20/2018

Level	a_M	a_L	k	Adjusted R^2 (%)
A	1.07 ± 0.09	−0.30 ± 0.10	0.79 ± 0.05	86.14
B	1.11 ± 0.07	−0.38 ± 0.06	0.75 ± 0.03	84.83
C	0.64 ± 0.11	−0.27 ± 0.11	0.59 ± 0.10	48.36
D	−0.43 ± 0.06	0.26 ± 0.04	1.66 ± 0.18	93.93

Table 2. Model of the variation of $\hat{s}_M$ and $\hat{s}_L$ with background wavelength at Levels A to D. *Note*: Best-fitting parameters and ±standard error of the fitted parameter and adjusted R^2.

of the form common at Levels A and B to the different form found at Level D.

How might we account for the dependence of $\hat{s}_M$ and $\hat{s}_L$ on background wavelength? Figure 11 illustrates a working model proposed for the underlying pathways. The red and green triangles in Figure 11 represent the L- and M-cones, respectively, and the orange ellipses represent horizontal cells. The central triangles, labelled "Local center," show M- and L-cone types summing to produce the achromatic signal. (Throughout the circuitry, we show two L-cones and one M-cone, since, on average, L-cones outnumber M-cones by two-to-one in normal retinae; e.g., Cicerone & Nerger, 1989; Vimal et al., 1989; Carroll et al., 2002; Hofer et al., 2005; Sharpe et al., 2011) but typically details for only one of the two L-cones are shown.) For clarity of description, we call the central cones the "principal" cones, since it is their response that represents the fast L- and M-cone inputs ($+fL$ and $+fM$) in the diagram, but note that all the cones in the diagram contribute fast signals. Each of the principal cones is connected to a local horizontal cell which receives input from two L-cones and an M-cone that provide the principal cone's surround, and have delays of between 2 and 9 ms (Lee et al., 1989a; Smith et al., 1992; Lee et al., 1994; Benardete & Kaplan, 1997). Note that these very short delays cannot account for the 29-ms delays seen in our data, and, being antagonistic to the principal cones, are likely to reduce the amplitude of the fast signal without substantially changing its timing, so they do not feature in our modelling. They are noted as $-f'M$ and $-f'L$ in the diagram. The local horizontal cells are in turn connected to more distant horizontal cells via synergistic gap junctions (Packer & Dacey, 2002, 2005) with an effective delay of Δt, as indicated in the diagram, and (depending on the version of the model) a low-pass filter represented in the diagram by an exponential decay.

These second-level horizontal cells also contact two L-cones and one M-cone, each of which contact a further horizontal cell. However, the lateral connections to the third-level horizontal cells are *local* connections. (The small negative sign and accompanying black rectangle, expanded in the inset panel at the bottom of the figure, represents an additional delay and a sign inversion in the local surround feedback.) We assume that signals from the surrounds are subject to an additional delay because of the extra synaptic steps. In various versions of our models, this additional delay is between about 2 and 5 ms (see Table 1 and Figure 7), and is consistent with the center-surround delays expected of parvocellular ganglion cells (Lee et al., 1989a; Smith et al., 1992; Lee et al., 1994; Benardete & Kaplan, 1997).

In the model, we assume that the cones that connect to the principal cones though only one delay and, possibly one low-pass filter, produce the $-sL$ and $-sM$ signals, whereas the cones that connect with the principal cones indirectly through the local surrounds produce, because of the double inversion, the slightly delayed $+sM$ and $+sL$ signals. Thus, the slow $+sM$ and $-sL$ signals are actually $-s(L - M)$ and the slow $+sL$ and $-sM$ signals are actually $-s(M - L)$.

We assume that for equichromatic flicker the slow $-sL$, $-sM$, $+sM$, and $+sL$ signals largely cancel each other in the distant surround networks, so that the predominant output signals are $+fM$ and $+fL$. Although selective chromatic adaptation changes the balance of the $-sM{+}sL$ and $+sM{-}sL$ signals, the slow signals are still cancelled for equichromatic flicker, because $|-sM| \approx +sL$ and $+sM \approx |-sL|$. However, for cone-isolating flicker there is an imbalance between the $-sM$ and $+sM$ signals and between the $-sL$ and $+sL$ signals, so that one of the two predominates. The idea that chromatic M-L and L-M parvocellular signals cancel each other in magnocellular pathways was discussed by Lee and Sun (2009).

Selective cone adaptation, which depends on the relative M- and L-cone excitation and thus on the spectral sensitivities of the cones, is assumed to attenuate one of the cone signals relative to the other; which cone is attenuated depends on the background wavelength and the amount of attenuation, and on the background intensity. On middle-wavelength backgrounds, on which the M- and L-cone excitation is more equal, the $+sM{-}sL$ and $-sM{+}sL$ will be balanced and will therefore be smaller because the $-sM$ and $+sM$ will cancel as will the $-sL$ and $+sL$ signals. In terms of Equation 7, the signals are balanced at the background wavelength (λ) when $M(\lambda)/L(\lambda) = k$.

For shorter-wavelength adaptation, for which the excitation of M > L, signals through the M-cones are more attenuated, whereas for low and moderate intensity long-wavelength adaptation, for which the excitation of L > M, signals through the L-cones are more attenuated. As highlighted by the blue areas of Figure 11, on shorter wavelength backgrounds signals through L-cones are favoured (i.e., $+sM{-}sL$), whereas as highlighted by the red areas, on low and moderate intensity longer wavelength fields, signals through M-cones are favoured (i.e., $-sM{+}sL$). In terms of Equation 7, on shorter wavelength backgrounds for which $M(\lambda)/L(\lambda){>}k$, $\hat{s}_M(\lambda)$ increases and $\hat{s}_L(\lambda)$ de-

Downloaded From: http://jov.arvojournals.org/pdfaccess.ashx?url=/data/journals/jov/936743/ on 02/20/2018

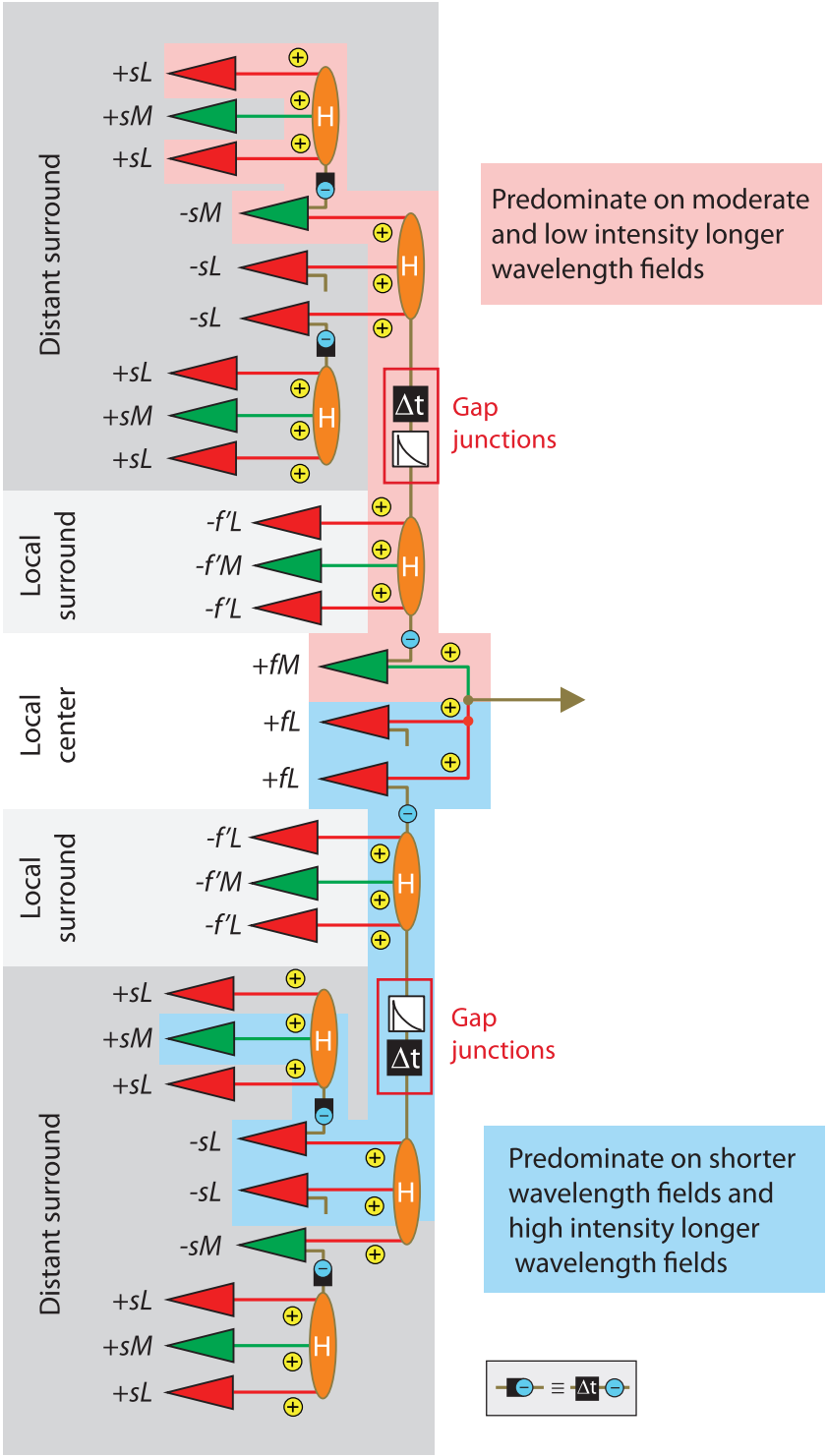

Figure 11. Schematic illustration of an explanatory model of the pathways underlying the slow and fast cone signals. M and L cones are represented by red and green triangles, respectively, and horizontal cells by the orange ellipses labelled H. Excitatory connections are shown by the yellow + signs, and inhibitory ones by blue − signs. The connections are relative to the three principal cones in the center of the diagram that make up the local center, labelled $+fM$ and $+fL$, the outputs of which are assumed to feed into the luminance or magnocellular pathway. The local surround cones, the feedback from which is mediated by horizontal cells, are labelled $-f'M$ and $-f'L$. The distant surround cones feedback via a delay (Δt) and a low-pass filter (represented by an exponential delay following an impulse) that we assume correspond to synergistic gap-junction connections between local and distant horizontal cells. The first level of distant surround cones, labelled $-sM$ and $-sL$, are inhibitory because they feedback through a single inhibitory →

Downloaded From: http://jov.arvojournals.org/pdfaccess.ashx?url=/data/journals/jov/936743/ on 02/20/2018

←

synapse. The second level of distant surround cones, labelled $+sM$ and $+sL$, make up the local surround of $-sM$ and $-sL$ cones. They are excitatory by virtue of passing through two inhibitory synapses, and are subject to slightly longer delays than the $-sM$ and $-sL$ signals because of the local surround feedback. $+sM-sL$ signals predominate on short-wavelength and high-intensity long-wavelength background fields (blue highlights), whereas $-sM+sL$ signals predominate on low- and moderate-intensity long-wavelength fields. Twice as many L-cones are shown than M-cones, which is consistent with their mean relative number in normal retinae.

creases above and below zero, respectively, according to the ratio $M(\lambda)/L(\lambda)$. On longer wavelength backgrounds for which $M(\lambda)/L(\lambda) < k$, $\hat{s}_M(\lambda)$ decreases and $\hat{s}_L(\lambda)$ increases below and above, respectively, also according to $M(\lambda)/L(\lambda)$.

On longer-wavelength fields, the change in predominance from $-sM+sL$ signals on low and moderate intensities background fields to $+sM-sL$ signals on high intensity fields is likely to be due to the effects of L-cone photopigment bleaching's changing the effective ratio of M- to L-cone excitations from M < L at low intensities to M > L at high intensities, such that physiologically the red field becomes effectively green. (This transition and a model related to the one shown in Figure 11 were proposed in 2006 and discussed in detail in Stockman & Plummer, 2005a.) Indeed, at very high intensities, the hue of a long-wavelength field gradually changes from red to yellow and finally to green, which remains the steady-state appearance (Auerbach & Wald, 1955; Cornsweet et al., 1958).

Note that in the model illustrated in Figure 11 we assume that the important local surround signals from third-level cones are from cones of the opposite sign (Reid & Shapley, 1992; Lee, Kremers, & Yeh, 1998; Reid & Shapley, 2002), but the surround signals could also be mixed, as might be expected from the anatomy (e.g., Kolb & Dekorver, 1991; Calkins, Schein, Tsukamoto, & Sterling, 1994). Note also that although in the model we show the processing as sequential from third-level cone to second-level cone to principal cone, the processing is of course recursive, since each cone is simultaneously a principal cone, a second-level cone, and a third-level cone. One important consequence of this is that the local feedback *within* a cone must be different with respect to its output to parvocellular bipolar cells and its output to magnocellular bipolar cells. For example, achromatic or equichromatic flickering lights that cover the local surround of a given M- or L-cone produce a small signal in that cone's output to a parvocellular bipolar because the surround feedback signals balance the cone output signal. Yet that same cone with the same local feedback must simultaneously produce a strong output to a magnocellular bipolar cell, otherwise the luminance flicker would be invisible. Thus, the local circuitry in the cone pedicle must be different for the midget and diffuse cone to cone bipolar synapses (see, e.g., Haverkamp, Grunert, & Wassle, 2000) either in terms of feedback weights or in terms of the transient or sustained nature of the feedback.

Concluding remarks

We have been able predict an extensive set of M- L-cone phase measurements made on a variety of different background wavelengths and radiances with a remarkably simple model. We find evidence for multiple M- and L-cone inputs to the so-called luminance channel, which we characterize as either slow ($+sM-sL$ or $+sL-sM$) and fast ($+fM+fL$). Both types of signal feed into a common achromatic channel, and contribute to flicker nulls. These signals are present under most conditions, but since the $+sM-sL$ or $+sL-sM$ signals are opposite in phase, they cancel each other; but we have shown that under particular sets of conditions one or the other predominates. Under most natural conditions, which rarely involve cone-isolating lights or strong chromatic adaptation, the $+sM-sL$ and $+sL-sM$ signals in the achromatic channel are probably small, *because* they cancel each other. The transition from predominance of $+sL-sM$ to predominance of $+sM-sL$ occurs as the adapting background field changes from long to short-wavelengths, or as the intensity of the adapting field is made very intense.

The results of this work have important consequences for experiments that rely on equiluminant stimuli to probe the properties of chromatic channels. The existence of sluggish "chromatic" inputs to the achromatic channel means that the results of experiments carried out at equiluminance are equivocal, since instead of just stimulating the chromatic channel, such stimuli also stimulate the slow inputs to the achromatic channel. Many of the unusual properties of perception at equiluminance could be the result of the slow inputs to the achromatic channel rather than to the behavior of chromatic channels per se.

Keywords: color vision, red cones, green cones, middle-wavelength sensitive cones, long-wavelength sensitive cones, flicker Sensitivity and phase difference, luminance, chromatic

Acknowledgments

This work was supported by BBSRC grants BB/1003444/1 and BB/M00211X/1.

Commercial relationships: none.

Downloaded From: http://jov.arvojournals.org/pdfaccess.ashx?url=/data/journals/jov/936743/ on 02/20/2018

Corresponding author: Andrew Stockman.
Email: a.stockman@ucl.ac.uk.
Address: UCL Institute of Ophthalmology, University College London, London, UK.

This paper is dedicated to the memory of Daniel J. Plummer.

References

Ahnelt, P. K., & Kolb, H. (1994). Horizontal cells and cone photoreceptors in primate retina: A Golgi-light microscope study of spectral connectivity. *Journal of Comparative Neurology*, *343*, 387–405.

Auerbach, E., & Wald, G. (1955). The participation of different types of cones in human light and dark adaptation. *American Journal of Ophthalmology*, *39*(2 Pt. 2), 24–40.

Baylor, D. A., Fuortes, M. G., & O'Bryan, P. M. (1971). Receptive fields of cones in the retina of the turtle. *Journal of Physiology*, *214*(2), 265–294.

Benardete, E. A., & Kaplan, E. (1997). The receptive field of primate P retinal ganglion cell, I: Linear dynamics. *Visual Neuroscience*, *14*(1), 169–185.

Boycott, B. B., & Dowling, J. E. (1969). Organisation of the primate retina: Light microscopy. *Philosophical Transactions of the Royal Society of London. Series B*, *255*, 109–184.

Boycott, B. B., Hopkins, J. M., & Sperling, H. G. (1987). Cone connections of the horizontal cells of the rhesus monkey's retina. *Proceedings of the Royal Society of London. Series B*, *229*(1257), 345–379.

Boycott, B. B., & Wässle, H. (1991). Morphological classification of bipolar cells of the primate retina. *European Journal of Neuroscience*, *3*(11), 1069–1088.

Boynton, R. M. (1979). *Human color vision*. New York, NY: Holt, Rinehart and Winston.

Calkins, D. J., Schein, S. J., Tsukamoto, Y., & Sterling, P. (1994). M and L cones in macaque fovea connect to midget ganglion cells by different numbers of excitatory synapses. *Nature*, *371*(6492), 70–72.

Calkins, D. J., & Sterling, P. (2007). Microcircuitry for two types of achromatic ganglion cell in primate fovea. *Journal of Neuroscience*, *27*(10), 2646–2653.

Calkins, D. J., Tsukamato, Y., & Sterling, P. (1996). Foveal cones form basal as well as invaginating junctions with diffuse ON bipolar cells. *Vision Research*, *36*(21), 3373–3381.

Campbell, F. W., Rothwell, S. E., & Perry, M. J. (1987). Bad light stops play. *Ophthalmic and Physiological Optics*, *7*(2), 165–167.

Carroll, J., Neitz, J., & Neitz, M. (2002). Estimates of L:M cone ratio from ERG flicker photometry and genetics. *Journal of Vision*, *2*(8):1, 531–542, doi:10.1167/2.8.1. [PubMed] [Article]

Cicerone, C. M., & Nerger, J. L. (1989). The relative numbers of long-wavelength-sensitive to middle-wavelength-sensitive cones in the human fovea centralis. *Vision Research*, *29*(1), 115–128.

Cornsweet, T. N., Fowler, H., Rabedeau, R. G., Whalen, R. E., & Williams, D. R. (1958). Changes in the perceived color of very bright stimuli. *Science*, *128*(3329), 898–899.

Cushman, W. B., & Levinson, J. Z. (1983). Phase shift in red and green counter-phase flicker at high frequencies. *Journal of the Optical Society of America*, *73*, 1557–1561.

Dacey, D. M., Lee, B. B., Stafford, D. K., Pokorny, J., & Smith, V. C. (1996). Horizontal cells of the primate retina: Cone specificity without spectral opponency. *Science*, *271*(5249), 656–659.

Dacheux, R. F., & Raviola, E. (1990). Physiology of H1 horizontal cells in the primate retina. *Proceedings of the Royal Society of London. Series B*, *239*, 213–230.

de Lange, H. (1958). Research into the dynamic nature of the human fovea-cortex systems with intermittent and modulated light. II. Phase shift in brightness and delay in color perception. *Journal of the Optical Society of America*, *48*, 784–789.

Eisner, A., & MacLeod, D. I. A. (1980). Blue sensitive cones do not contribute to luminance. *Journal of the Optical Society of America*, *70*, 121–123.

Gielen, C. C. A. M., van Gisbergen, J. A. M., & Vendrik, A. J. H. (1982). Reconstruction of cone-system contributions to responses of colour-opponent neurones in monkey lateral geniculate. *Biological Cybernetics*, *44*(3), 211–221.

Goodchild, A. K., Chan, T. L., & Grünert, U. (1996). Horizontal cell connections with short-wavelength-sensitive cones in macaque monkey retina. *Visual Neuroscience*, *13*(5), 833–845.

Gouras, P., & Eggers, H. (1983). Responses of primate retinal ganglion cells to moving spectral contrast. *Vision Research*, *23*(10), 1175–1182.

Gouras, P., & Zrenner, E. (1979). Enhancement of luminance flicker by color-opponent mechanisms. *Science*, *205*(4406), 587–589.

Guth, S. L., Alexander, J. V., Chumbly, J. I., Gillman, C. B., & Patterson, M. M. (1968). Factors affecting

Downloaded From: http://jov.arvojournals.org/pdfaccess.ashx?url=/data/journals/jov/936743/ on 02/20/2018

luminance additivity at threshold among normal and color-blind subjects and elaborations of a trichromatic-opponent color theory. *Vision Research*, *8*(7), 913–928.

Haverkamp, S., Grunert, U., & Wassle, H. (2000). The cone pedicle, a complex synapse in the retina. *Neuron*, *27*(1), 85–95.

Hofer, H. J., Carroll, J., Neitz, J., Neitz, M., & Williams, D. R. (2005). Organization of the human trichromatic cone mosaic. *Journal of Neuroscience*, *25*(42), 9669–9679.

Ives, H. E. (1923). A chart of the flicker photometer. *Journal of the Optical Society of America*, *7*(5), 363–373.

Jacoby, R. A., Stafford, D., Kouyama, N., & Marshak, D. (1996). Synaptic inputs to ON parasol ganglion cells in the primate retina. *Journal of Neuroscience*, *16*(24), 8041–8056.

Jacoby, R. A., Wiechmann, A. F., Amara, S. G., Leighton, B. H., & Marshak, D. W. (2000). Diffuse bipolar cells provide input to OFF parasol ganglion cells in the macaque retina. *Journal of Comparative Neurology*, *416*(1), 6–18.

Kolb, H., & Dekorver, L. (1991). Midget ganglion cells of the parafovea of the human retina: A study by electron microscopy and serial reconstructions. *Journal of Comparative Neurology*, *303*(4), 617–636.

Kraft, T. W., Neitz, J., & Neitz, M. (1998). Spectra of human L cones. *Vision Research*, *38*(23), 3663–3670.

Kremers, J., Yeh, T., & Lee, B. B. (1993). The response of macaque ganglion cells and human observers to heterochromatically modulated lights: The effect of stimulus size. *Vision Research*, *34*, 217–221.

Kvalseth, T. O. (1985). Cautionary note about R^2. *The American Statistician*, *39*(4), 279–285.

Lee, B. B., Kremers, J., & Yeh, T. (1998). Receptive fields of primate retinal ganglion cells studied with a novel technique. *Visual Neuroscience*, *15*(1), 161–175.

Lee, B. B., Martin, P. R., & Valberg, A. (1988). The physiological basis of heterochromatic flicker photometry demonstrated in the ganglion cells of the macaque retina. *Journal of Physiology*, *404*, 323–347.

Lee, B. B., Martin, P. R., & Valberg, A. (1989a). Amplitude and phase of responses of macaque retinal ganglion cells to flickering stimuli. *Journal of Physiology*, *414*, 245–263.

Lee, B. B., Martin, P. R., & Valberg, A. (1989b). Nonlinear summation of M- and L-cone inputs to phasic retinal ganglion cells of the macaque. *Journal of Neuroscience*, *9*(4), 1433–1442.

Lee, B. B., Pokorny, J., Smith, V. C., & Kremers, J. (1994). Responses to pulses and sinusoids in macaque ganglion cells. *Vision Research*, *34*(23), 3081–3096.

Lee, B. B., Pokorny, J., Smith, V. C., Martin, P. R., & Valberg, A. (1990). Luminance and chromatic modulation sensitivity of macaque ganglion cells and human observers. *Journal of the Optical Society of America A*, *7*(12), 2223–2236.

Lee, B. B., & Sun, H. (2004). Chromatic input to cells of the magnocellular pathway: Mean chromaticity and the relative phase of modulated lights. *Visual Neuroscience*, *21*(3), 309–314.

Lee, B. B., & Sun, H. (2009). The chromatic input to cells of the magnocellular pathway of primates. *Journal of Vision*, *9*(2):15, 1–18, doi:10.1167/9.2.15. [PubMed] [Article]

Lee, J., & Stromeyer, C. F., III. (1989). Contribution of human short-wave cones to luminance and motion detection. *Journal of Physiology*, *413*, 563–593.

Lennie, P., Pokorny, J., & Smith, V. C. (1993). Luminance. *Journal of the Optical Society of America A*, *10*(6), 1283–1293.

Levenberg, K. (1944). A method for the solution of certain non-linear problems in least squares. *Quarterly of Applied Mathematics*, *2*(2), 164–168.

Leventhal, A. G., Rodieck, R. W., & Dreher, B. (1981). Retinal ganglion-cell classes in the old-world monkey—morphology and central projections. *Science*, *213*(4512), 1139–1142.

Lindsey, D. T., Pokorny, J., & Smith, V. C. (1986). Phase-dependent sensitivity to heterochromatic flicker. *Journal of the Optical Society of America A*, *3*(7), 921–927.

Livingstone, M. S., & Hubel, D. H. (1987). Psychophysical evidence for separate channels for the perception of form, colour, movement and depth. *Journal of Neuroscience*, *7*(11), 3416–3468.

Luther, R. (1927). Aus dem gebiet der farbreizmetrik [On color stimulus metrics]. *Zeitschrift für technische Physik*, *8*, 540–558.

Mariani, A. P. (1981). A diffuse, invaginating cone bipolar cell in primate retina. *Journal of Comparative Neurology*, *197*(4), 661–671.

Marquardt, D. W. (1963). An algorithm for least-squares estimation of nonlinear parameters. *Journal of the Society for Industrial and Applied Mathematics*, *11*(2), 431–441.

Merbs, S. L., & Nathans, J. (1992). Absorption spectra of human cone pigments. *Nature*, *356*, 431–432.

Mitchell, D. E., & Rushton, W. A. H. (1971). Visual

Downloaded From: http://jov.arvojournals.org/pdfaccess.ashx?url=/data/journals/jov/936743/ on 02/20/2018

pigments in dichromats. *Vision Research*, *11*(10), 1033–1043.

Packer, O. S., & Dacey, D. M. (2002). Receptive field structure of H1 horizontal cells in macaque monkey retina. *Journal of Vision*, *2*(4):1, 272–292, doi:10.1167/2.4.1. [PubMed] [Article]

Packer, O. S., & Dacey, D. M. (2005). Synergistic center-surround receptive field model of monkey H1 horizontal cells. *Journal of Vision*, *5*(11):9, 1038–1054, doi:10.1167/5.11.9. [PubMed] [Article]

Perry, V. H., Oehler, R., & Cowey, A. (1984). Retinal ganglion cells that project to the dorsal lateral geniculate nucleus in the macaque monkey. *Neuroscience*, *12*(4), 1101–1123.

Polyak, S. L. (1941). *The retina*. Chicago: University of Chicago.

Pugh, E. N., Jr. (1988). Vision: Physics and retinal physiology. In R. C. Atkinson, R. J. Herrnstein, G. Lindsey, & R. D. Luce (Eds.), *Stevens' handbook of experimental psychology*, (2nd ed., Vol. 1, pp. 75–163). New York, NY: Wiley.

Reid, R. C., & Shapley, R. M. (1992). Spatial structure of cone inputs to the receptive fields in primate lateral geniculate nucleus. *Nature*, *356*(6371), 716–718.

Reid, R. C., & Shapley, R. M. (2002). Space and time maps of cone photoreceptor signals in macaque lateral geniculate nucleus. *Journal of Neuroscience*, *22*(14), 6158–6175.

Ripamonti, C., Woo, W. L., Crowther, E., & Stockman, A. (2009). The S-cone contribution to luminance depends on the M- and L-cone adaptation levels: Silent surrounds? *Journal of Vision*, *9*(3): 10, 1–16, doi:10.1167/9.3.10. [PubMed] [Article]

Rodieck, R. W., Binmoeller, K. F., & Dineen, J. (1985). Parasol and midget ganglion-cells of the human retina. *Journal of Comparative Neurology*, *233*(1), 115–132.

Rogers, B. J., & Anstis, S. M. (1972). Intensity versus adaptation and the Pulfrich stereophenomenon. *Vision Research*, *12*(5), 909–928.

Schiller, P. H., & Colby, C. L. (1983). The responses of single cells in the lateral geniculate nucleus of the rhesus monkey to color and luminance contrast. *Vision Research*, *23*(12), 1631–1641.

Schrödinger, E. (1925). Über das verhältnis der vierfarben zur dreifarbentheorie [On the relation between the four-colour and the three-colour theory]. *Sitzungberichte. Abt. 2a, Mathematik, Astronomie, Physik, Meteorologie und Mechanik. Akademie der Wissenschaften in Wien, Mathematisch-Naturwissenschaftliche Klasse*, *134*, 471–490.

Sharpe, L. T., Stockman, A., Jagla, W., & Jägle, H. (2005). A luminous efficiency function, V*(λ), for daylight adaptation. *Journal of Vision*, *5*(11):3, 948–968, doi:10.1167/5.11.3. [PubMed] [Article]

Sharpe, L. T., Stockman, A., Jagla, W., & Jägle, H. (2011). A luminous efficiency function, $V^*_{D65}(\lambda)$, for daylight adaptation: A correction. *Color Research & Application*, *36*, 42–46.

Sharpe, L. T., Stockman, A., Jägle, H., Knau, H., Klausen, G., Reitner, A., & Nathans, J. (1998). Red, green, and red-green hybrid photopigments in the human retina: Correlations between deduced protein sequences and psychophysically-measured spectral sensitivities. *Journal of Neuroscience*, *18*, 10053–10069.

Smith, V. C., Lee, B. B., Pokorny, J., Martin, P. R., & Valberg, A. (1992). Responses of macaque ganglion cells to the relative phase of heterochromatically modulated lights. *Journal of Physiology*, *458*, 191–221.

Smith, V. C., & Pokorny, J. (1975). Spectral sensitivity of the foveal cone photopigments between 400 and 500 nm. *Vision Research*, *15*, 161–171.

Smith, V. C., Pokorny, J., Lee, B. B., & Dacey, D. M. (2001). Primate horizontal cell dynamics: An analysis of sensitivity regulation in the outer retina. *Journal of Neurophysiology*, *85*(2), 545–558.

Spiess, A.-N., & Neumeyer, N. (2010). An evaluation of R^2 as an inadequate measure for nonlinear models in pharmacological and biochemical research: A Monte Carlo approach. *BMC Pharmacology, 10*, *6*, 1–11.

Stockman, A. (2001). Multiple cone inputs to luminance. *Investigative Ophthalmology and Visual Science (supplement)*, *42*(4), S320.

Stockman, A. (2013). Cone signals feeding into luminance can exhibit large phase delays and sign reversals: The effect of an inhibitory surround network? *Investigative Ophthalmology & Visual Science*, *54*(15), 3710. Abstract retrieved from http://iovs.arvojournals.org/article.aspx?articleid=2148518

Stockman, A., Henning, G. B., & Rider, A. T. (2017). Linear-nonlinear models of the red-green chromatic pathway. *Journal of Vision*, *17*(13):7, doi:10.1167/17.13.7. [PubMed] [Article]

Stockman, A., Langendörfer, M., Smithson, H. E., & Sharpe, L. T. (2006). Human cone light adaptation: From behavioral measurements to molecular mechanisms. *Journal of Vision*, *6*(11):5, 1194–1213, doi:10.1167/6.11.5. [PubMed] [Article]

Stockman, A., MacLeod, D. I. A., & DePriest, D. D. (1987). An inverted S-cone input to the luminance channel: Evidence for two processes in S-cone

Downloaded From: http://jov.arvojournals.org/pdfaccess.ashx?url=/data/journals/jov/936743/ on 02/20/2018

flicker detection. *Investigative Ophthalmology and Visual Science*, *28*(Suppl.), 92.

Stockman, A., MacLeod, D. I. A., & DePriest, D. D. (1991). The temporal properties of the human short-wave photoreceptors and their associated pathways. *Vision Research*, *31*(2), 189–208.

Stockman, A., MacLeod, D. I. A., & Lebrun, S. (1993). Faster than the eye can see: Blue cones respond to rapid flicker. *Journal of the Optical Society of America A*, *10*(6), 1396–1402.

Stockman, A., Montag, E. D., & MacLeod, D. I. A. (1991). Large changes in phase delay on intense bleaching backgrounds. *Investigative Ophthalmology and Visual Science*, *32*(Suppl. 4), 841.

Stockman, A., Montag, E. D., & Plummer, D. J. (2006). Paradoxical shifts in human colour sensitivity caused by constructive and destructive interference between signals from the same cone class. *Visual Neuroscience*, *23*(3–4), 471–478.

Stockman, A., & Plummer, D. J. (1994). The luminance channel can be opponent?? *Investigative Ophthalmology and Visual Science*, *35*(4), 1572.

Stockman, A., & Plummer, D. J. (1998). Color from invisible flicker: A failure of the Talbot-Plateau law caused by an early "hard" saturating nonlinearity used to partition the human short-wave cone pathway. *Vision Research*, *38*(23), 3703–3728.

Stockman, A., & Plummer, D. J. (2005a). Long-wavelength adaptation reveals slow, spectrally-opponent inputs to the human luminance pathway. *Journal of Vision*, *5*(9):5, 702–716, doi:10.1167/5.9.5. [PubMed] [Article]

Stockman, A., & Plummer, D. J. (2005b). Spectrally-opponent inputs to the human luminance pathway: Slow +L and -M cone inputs revealed by low to moderate long-wavelength adaptation. *Journal of Physiology*, *566*(Pt. 1), 77–91.

Stockman, A., Plummer, D. J., & Montag, E. D. (2005). Spectrally-opponent inputs to the human luminance pathway: Slow +M and -L cone inputs revealed by intense long-wavelength adaptation. *Journal of Physiology*, *566*(Pt. 1), 61–76.

Stockman, A., & Sharpe, L. T. (2000). Spectral sensitivities of the middle- and long-wavelength sensitive cones derived from measurements in observers of known genotype. *Vision Research*, *40*(13), 1711–1737.

Stromeyer, C. F., III, Chaparro, A., Tolias, A. S., & Kronauer, R. E. (1997). Colour adaptation modifies the long-wave versus middle-wave cone weights and temporal phases in human luminance (but not red-green) mechanism. *Journal of Physiology*, *499*, 227–254.

Stromeyer, C. F., III, Gowdy, P. D., Chaparro, A., Kladakis, S., Willen, J. D., & Kronauer, R. E. (2000). Colour adaptation modifies the temporal properties of the long- and middle-wave cone signals in the human luminance mechanism. *Journal of Physiology*, *526*, 177–194.

Swanson, W. H., Pokorny, J., & Smith, V. C. (1987). Effects of temporal frequency on phase-dependent sensitivity to heterochromatic flicker. *Journal of the Optical Society of America A*, *4*(12), 2266–2273.

Thoreson, W. B., & Mangel, S. C. (2012). Lateral interactions in the outer retina. *Progress in Retinal and Eye Research*, *31*(5), 407–441.

Troland, L. T. (1916). Notes on flicker photometry: Flicker-photometer frequency as a function of the color of the standard, and of the measured, light. *Journal of the Franklin Institute*, *181*(6), 853–855.

Van De Grind, W. A., Grüsser, O. J., & Lunkenheimer, H. U. (1973). Temporal transfer properties of the afferent visual system psychophysical, neurophysiological and theoretical investigations. In R. Jung (Ed.), *Central processing of visual information A: Integrative functions and comparative data* (Vol. VII/3A, pp. 431–573): Berlin and Heidelberg, Germany: Springer.

Vimal, R. L. P., Smith, V. C., Pokorny, J., & Shevell, S. K. (1989). Foveal cone thresholds. *Vision Research*, *29*(1), 61–78.

von Grünau, M. W. (1977). Lateral interactions and rod intrusions in color flicker. *Vision Research*, *17*, 911–916.

Walls, G. L. (1955). A branched-pathway schema for the color-vision system and some of the evidence for it. *American Journal of Ophthalmology*, *39*(2), 8–23.

Walraven, P. L., & Leebeek, H. J. (1964). Phase shift of sinusoidally alternating colored stimuli. *Journal of the Optical Society of America*, *54*, 78–82.

Werblin, F. S., & Dowling, J. E. (1969). Organization of the retina of the mudpuppy, Necturus maculosus. II. Intracellular recording. *Journal of Neurophysiology*, *32*(3), 339–355.

Westheimer, G. (1966). The Maxwellian view. *Vision Research*, *6*(12), 669–682.

Yeh, T., Lee, B. B., & Kremers, J. (1995). Temporal response of ganglion cells of the macaque retina to cone-specific modulation. *Journal of the Optical Society America A*, *12*(3), 456–464.

Downloaded From: http://jov.arvojournals.org/pdfaccess.ashx?url=/data/journals/jov/936743/ on 02/20/2018

Appendix

Appendix 1: Experimental conditions

DJP	Background			M target radiances (L-equated)		L target radiances (M-equated)	
Background wavelength	Radiance	Retinal illuminance	Equichromatic target radiance	540 nm	650 nm	650 nm	550 nm
410 nm							
A*	9.76	0.88	7.77	6.41	7.21	7.41	5.54
B	10.97	2.09	9.72	8.44	9.24	9.18	7.31
440 nm							
A*	9.10	1.47	7.59	6.45	7.25	7.41	5.54
B	10.28	2.65	8.95	7.74	8.54	8.48	6.61
C	11.46	3.83	10.1	8.92	9.72	9.78	7.91
469 nm							
A*	9.06	1.98	7.55	6.75	7.70	7.71	5.84
B	9.95	2.87	8.64	8.25	9.05	8.42	6.55
C	11.12	4.04	9.71	8.88	9.83	9.78	7.91
491 nm							
A*	8.54	1.83	6.83	6.41	7.21	7.41	5.54
B	9.76	3.05	8.41	7.81	8.61	8.68	6.81
C	10.88	4.17	9.32	8.88	9.68	9.78	7.91
520 nm							
A*	8.11	1.89	6.75	6.41	7.21	7.41	5.54
B	9.29	3.07	8.00	7.78	8.58	8.69	6.82
C	10.40	4.18	8.97	9.00	9.80	9.63	7.76
D	11.56	5.34	10.59	10.05	10.85	11.13	9.26
550 nm							
A*	8.01	1.92	6.62	6.41	7.21	7.41	5.54
B	9.14	3.05	7.84	7.78	8.58	8.69	6.82
C	10.27	4.18	8.87	8.99	9.79	9.87	8.00
D	11.49	5.40	10.18	10.04	10.84	11.12	9.25
578 nm							
A*	8.08	1.92	6.87	6.41	7.21	7.41	5.54
B	9.25	3.09	8.01	7.93	8.73	8.72	6.85
C	10.49	4.33	9.05	9.35	10.15	10.13	8.25
D	11.53	5.37	10.22	10.05	10.85	11.13	9.26
600 nm							
A*	8.01	1.63	6.62	6.41	7.21	7.41	5.54
B	9.40	3.07	8.15	8.00	8.80	9.02	7.15
C	10.62	4.29	9.42	9.22	10.02	10.26	8.39
D	11.59	5.26	10.39	10.17	10.97	11.11	9.24
633 nm							
A*	8.20	1.42	6.88	6.41	7.21	7.41	5.54
B	9.42	2.64	8.27	7.51	8.31	8.85	6.98
C	10.65	3.87	9.25	8.21	9.01	9.83	7.97
D	11.91	5.13	10.58	10.05	10.85	11.11	9.24
658 nm							
A*	8.98	1.65	8.28	6.99	7.79	8.10	6.23
B*	10.11	2.78	8.79	7.55	8.35	9.11	7.24
C++	11.29	3.96	9.81	8.33	9.13	9.85	7.98
D+	12.47	5.14	11.41	9.47	10.27	11.12	9.25

Table A1. Time-averaged stimulus radiances in $\log_{10}$ quanta s^{-1} deg^{-2} for each of the experimental conditions used for DJP, except column 3, which gives the background retinal illuminances in $\log_{10}$ photopic Td. *Notes*: Conditions marked by * were preceded by a 510-nm bleach of 12.25 $\log_{10}$ quanta s^{-1} deg^{-2} (5.89 $\log_{10}$ photopic Td) viewed for 3 s. For those marked by + or ++, an additional 410-nm auxiliary background of 10.80+ or 10.26++ $\log_{10}$ quanta s^{-1} deg^{-2} (1.92+ or 1.38++ $\log_{10}$ photopic Td) was added to suppress S-cones.

Downloaded From: http://jov.arvojournals.org/pdfaccess.ashx?url=/data/journals/jov/936743/ on 02/20/2018

SAA	Background			M target radiances (L-equated)		L target radiance (M-equated)	
Background wavelength	Radiance	Retinal illuminance	Equichromatic target radiance	540 nm	650 nm	650 nm	550 nm
410 nm							
B	11.27	2.39	9.72	8.44	9.39	9.18	7.31
440 nm							
B	10.27	2.64	8.69	7.74	8.69	8.48	6.61
469 nm							
A*	9.06	1.98	7.55	6.75	7.70	7.71	5.84
B	9.95	2.87	8.64	8.46	9.41	8.68	6.81
C	11.12	4.04	9.71	8.88	9.83	9.78	7.91
491 nm							
B	9.75	3.04	8.14	7.96	8.91	8.68	6.81
520 nm							
A*	8.10	1.88	6.75	7.01	7.96	7.71	5.84
B	9.29	3.07	8.00	7.78	8.73	8.69	6.82
C	10.40	4.18	8.97	9.00	9.95	9.63	7.76
D	11.56	5.34	10.59	9.95	10.9	11.05	9.18
550 nm							
B	9.14	3.05	7.76	7.93	8.88	8.69	6.82
578 nm							
A*	8.09	1.93	6.59	7.01	7.96	7.71	5.84
B	9.27	3.11	8.01	7.93	8.88	8.71	6.85
C	10.50	4.34	9.05	9.35	10.30	10.13	8.25
D	11.53	5.37	10.22	10.04	10.99	11.06	9.19
609 nm							
A	8.04	1.62	6.61	6.61	7.56	7.61	5.74
B	9.40	2.98	7.86	7.51	8.46	8.85	6.98
C	10.61	4.19	9.39	8.81	9.76	10.13	8.27
D	11.65	5.23	10.17	9.75	10.7	11.04	9.17
658 nm							
A*	8.98	1.65	8.28	6.99	7.94	8.10	6.23
B*	10.11	2.78	8.79	7.55	8.5	9.01	7.27
C++	11.28	3.95	10.07	8.46	9.31	10.01	8.14
D+	12.16	4.83	11.15	9.27	10.23	10.78	8.91

Table A2. Time-averaged stimulus radiances in $\log_{10}$ quanta s^{-1} deg^{-2} for each experimental condition used for SAA, except column 3 which gives the background retinal illuminances in $\log_{10}$ photopic Td. *Notes*: Conditions marked by * were preceded by a 510-nm bleach of 11.90 $\log_{10}$ quanta s^{-1} deg^{-2} (5.54 $\log_{10}$ photopic Td) viewed for 7 s. For those marked by + or ++, an additional 410-nm auxiliary background of 10.81+ or 10.31++ $\log_{10}$ quanta s^{-1} deg^{-2} (1.93+ or 1.43++ $\log_{10}$ photopic Td) was added to suppress the S-cones.

Downloaded From: http://jov.arvojournals.org/pdfaccess.ashx?url=/data/journals/jov/936743/ on 02/20/2018

RS	Background			M target radiances (L-equated)		L target radiances (M-equated)	
Background wavelength	Radiance	Retinal illuminance	Equichromatic target radiance	540 nm	650 nm	650 nm	550 nm
440 nm							
B	10.27	2.64	8.69	7.74	8.64	8.48	6.61
469 nm							
B	9.97	2.89	8.84	8.25	9.05	8.42	6.55
C	11.12	4.04	9.71	8.88	9.78	9.78	7.91
491 nm							
B	9.75	3.04	8.14	7.96	8.86	8.68	6.81
520 nm							
B	9.29	3.07	8.00	7.78	8.68	8.69	6.82
C	10.40	4.18	8.97	9.00	9.9	9.63	7.76
550 nm							
B	9.14	3.05	7.76	7.93	8.83	8.99	7.12
578 nm							
B	9.25	3.09	8.01	7.93	8.83	8.72	6.85
C	10.49	4.33	9.05	9.35	10.25	10.13	8.25
609 nm							
B	9.40	2.98	7.86	7.51	8.41	8.85	6.98
658 nm							
B*	10.11	2.78	8.79	7.55	8.45	9.11	7.24
C++	11.24	3.91	9.87	8.46	9.36	10.01	8.14
D+	12.17	4.84	11.15	9.27	10.17	10.78	8.91

Table A3. Time-averaged stimulus radiances in $\log_{10}$ quanta s^{-1} deg^{-2} for each of the experimental conditions used for RS, except column 3 which gives the background retinal illuminances in $\log_{10}$ photopic Td. *Notes*: Conditions marked by * were preceded by a 510-nm bleach of 11.90 $\log_{10}$ quanta s^{-1} deg^{-2} (5.54 $\log_{10}$ photopic Td) viewed for 7 s. For those marked by + or ++, an additional 410-nm auxiliary background of 10.80+ or 10.31++ $\log_{10}$ quanta s^{-1} deg^{-2} (1.92+ or 1.43++ $\log_{10}$ photopic Td) was added to suppress the S-cones.

Appendix 2: Model fits of the individually-fitted time delay model

AS	Background			M-cone target (L-cone equated)		L-cone target (M-cone equated)	
Background wavelength	Radiance	Retinal illuminance	Equichromatic target	540 nm	650 nm	650 nm	550 nm
410 nm							
B	11.07	2.19	9.96	8.60	9.40	9.20	7.33
469 nm							
B	9.98	2.90	8.64	8.46	9.26	8.68	6.81
520 nm							
C	10.39	4.17	9.13	9.14	9.94	9.67	8.10
578 nm							
C	10.49	4.33	9.05	9.35	10.15	10.13	8.25
600 nm							
C	10.38	4.05	9.15	8.90	9.70	10.09	8.19
658 nm							
B*	10.15	2.82	8.86	7.50	8.30	8.96	7.09
C++	11.21	3.88	9.86	8.44	9.24	10.00	8.13
D+	12.47	5.14	11.41	9.47	10.37	11.12	9.25

Table A4. Time-averaged stimulus radiances in $\log_{10}$ quanta s^{-1} deg^{-2} for each experimental condition used for AS, except column 4 which gives the background retinal illuminances in $\log_{10}$ photopic Td. *Notes*: Conditions marked by * were preceded by a 510-nm bleach of 12.22 $\log_{10}$ quanta s^{-1} deg^{-2} (5.86 $\log_{10}$ photopic Td) viewed for 3 s. For those marked by + or ++, an additional 410-nm auxiliary background of 10.80+ or 10.30++ $\log_{10}$ quanta s^{-1} deg^{-2} (1.92+ or 1.42++ $\log_{10}$ photopic Td) was added to suppress S-cones.

Downloaded From: http://jov.arvojournals.org/pdfaccess.ashx?url=/data/journals/jov/936743/ on 02/20/2018

DJP	M-cone target (L-cone equated)				L-cone target			
Background wavelength	$\hat{s}$	*SE*	Δt	*SE*	$\hat{s}$	*SE*	Δt	*SE*
410 nm								
A	0.33	0.02	30.68	1.20	−0.10	0.03	33.53	4.14
B	0.43	0.01	32.68	0.24	−0.09	0.03	37.76	3.70
440 nm								
A	0.84	0.11	30.19	2.31	−0.25	0.03	29.87	2.81
B	1.00	0.04	27.33	0.26	−0.25	0.02	26.19	1.20
C	0.34	0.01	46.52	0.78	−0.18	0.03	37.80	1.67
469 nm								
A	1.00	0.09	29.00	1.08	−0.23	0.03	28.65	3.14
B	0.95	0.03	27.59	0.26	−0.21	0.03	24.95	1.45
C	0.36	0.01	41.44	0.62	−0.27	0.02	36.43	1.14
491 nm								
A*	0.81	0.09	26.21	1.70	−0.50	186.76	0.01	633.79
B	1.00	0.04	26.41	0.27	−0.28	0.02	27.16	1.06
C	0.38	0.01	32.58	0.38	−0.16	0.03	31.20	2.36
520 nm								
A	0.42	0.01	32.67	0.40	−0.17	0.03	27.33	4.95
B	0.54	0.00	30.74	0.11	−0.21	0.03	28.39	1.55
C	0.36	0.01	34.76	0.54	−0.11	0.03	34.55	3.55
D	0.18	0.02	29.06	1.54	−0.10	0.03	32.49	3.83
550 nm								
A*	0.25	0.03	27.73	2.72	0.70	4909.28	1.37	9556.56
B	0.46	0.00	31.24	0.15	−0.23	0.03	27.98	1.41
C	0.34	0.01	33.69	0.57	−0.20	0.02	33.71	1.90
D	0.36	0.01	26.20	0.41	−0.13	0.03	24.63	2.36
578 nm								
A	−0.45	0.02	34.57	1.45	0.14	0.03	25.66	6.89
B	−0.46	0.01	21.59	0.62	0.23	0.02	22.77	0.83
C	0.45	0.00	32.33	0.19	−0.23	0.02	29.49	1.49
D	0.32	0.01	27.47	0.54	−0.13	0.03	33.18	3.12
600 nm								
A	−0.60	0.03	36.07	1.07	0.13	0.04	27.54	6.10
B	−0.63	0.02	23.89	0.44	0.36	0.01	23.44	0.36
C	0.70	0.02	34.84	0.26	−0.30	0.02	30.12	1.11
D	0.53	0.00	30.36	0.10	−0.27	0.02	30.24	1.24
633 nm								
A*	−0.54	0.02	32.92	1.26	0.66	40982.71	1.72	106349.93
B	−0.69	0.02	29.42	0.35	0.29	0.02	31.53	0.73
C	−0.60	0.02	22.00	0.49	0.41	0.01	22.08	0.24
D	0.78	0.02	36.91	0.28	−0.54	0.02	28.69	0.48
650 nm								
A	−0.63	0.02	32.70	0.54	0.03	0.04	28.92	11.21
B	−0.70	0.02	30.91	0.41	0.25	0.02	28.80	0.90
C	−0.79	0.03	22.76	0.38	0.16	0.03	21.50	1.50
D	0.97	0.04	33.56	0.28	−0.39	0.02	27.78	0.74

Table A5. Fits of the time-delay model to the data for DJP. The asterisks indicate rows in which the L-cone fits were highly uncertain; these fits were therefore not used for modeling (nor are they plotted in Figure 7). See text for further details.

Downloaded From: http://jov.arvojournals.org/pdfaccess.ashx?url=/data/journals/jov/936743/ on 02/20/2018

SAA	M-cone target (L-cone equated)				L-cone target			
Background wavelength	$\hat{s}$	*SE*	Δt	*SE*	$\hat{s}$	*SE*	Δt	*SE*
410 nm								
B	0.37	0.01	34.66	0.58	−0.09	0.04	23.36	3.94
440 nm								
B	0.99	0.05	23.15	0.34	−0.38	0.02	22.55	0.86
469 nm								
A	0.84	0.06	28.11	0.86	−0.52	0.01	25.11	0.81
B	0.90	0.04	24.78	0.29	−0.33	0.02	22.88	1.00
C	1.00	0.04	26.81	0.31	−0.37	0.02	21.89	0.91
491 nm								
B	1.00	0.05	23.81	0.33	−0.43	0.02	22.92	0.76
520 nm								
A	0.91	0.06	30.47	0.69	−0.07	0.04	22.90	13.32
B	1.00	0.05	25.07	0.32	−0.27	0.02	22.78	1.25
C	0.31	0.02	25.40	0.64	−0.14	0.03	21.31	2.63
D	0.19	0.03	30.45	1.66	−0.22	0.03	22.75	1.61
550 nm								
B	1.00	0.05	29.59	0.35	−0.18	0.03	32.21	2.47
578 nm								
A	−0.66	0.03	22.77	1.26	0.19	0.04	28.58	2.69
B	−0.56	0.02	20.82	0.61	0.13	0.03	25.28	2.29
C	0.45	0.01	22.80	0.18	−0.39	0.01	25.24	0.82
D	0.42	0.01	22.24	0.25	−0.29	0.02	22.52	1.18
609 nm								
A	−0.59	0.02	23.33	1.43	0.13	0.04	46.28	6.10
B	−0.61	0.02	21.42	0.55	0.31	0.02	23.63	0.58
C	0.50	0.01	25.00	0.18	−0.38	0.02	23.02	0.87
D	0.44	0.01	23.34	0.24	−0.44	0.01	22.03	0.74
658 nm								
A	−0.60	0.01	28.38	0.49	0.06	0.04	28.83	6.81
B	−0.78	0.03	25.82	0.39	0.31	0.02	24.23	0.61
C	−0.77	0.03	19.78	0.53	0.38	0.01	20.72	0.32
D	0.61	0.01	27.75	0.19	−0.54	0.01	22.73	0.59

Table A6. Fits of the time-delay model to the data for SA. See text for further details.

Downloaded From: http://jov.arvojournals.org/pdfaccess.ashx?url=/data/journals/jov/936743/ on 02/20/2018

RS	M-cone target (L-cone equated)				L-cone target			
Background wavelength	$\hat{s}$	*SE*	Δt	*SE*	$\hat{s}$	*SE*	Δt	*SE*
440 nm								
B	0.33	0.01	37.69	0.92	−0.15	0.03	27.95	2.25
469 nm								
B	1.00	0.04	28.99	0.26	−0.19	0.03	27.72	1.67
C	0.42	0.01	32.96	0.29	−0.14	0.03	27.44	2.37
491 nm								
B	0.58	0.01	40.34	0.27	−0.16	0.03	30.31	2.22
520 nm								
B	1.00	0.04	29.39	0.27	−0.11	0.03	33.09	3.69
C	0.42	0.01	33.16	0.29	−0.09	0.03	32.27	4.62
550 nm								
B*	0.27	0.02	35.76	0.93	0.49	137.95	1.45	412.77
578 nm								
B	−0.34	0.02	25.29	0.83	0.13	0.03	28.51	2.20
C	0.36	0.01	32.15	0.44	−0.13	0.03	31.04	3.03
609 nm								
B	−0.37	0.01	30.79	0.85	0.30	0.02	32.14	0.69
658 nm								
B	−0.52	0.01	35.89	0.52	0.34	0.01	33.52	0.56
C	−0.68	0.02	24.98	0.40	0.35	0.01	26.92	0.45
D	0.62	0.01	32.23	0.20	−0.33	0.02	31.26	0.99

Table A7. Fits of the time-delay model to the data for RS. The asterisk indicates a row in which the L-cone fits were highly uncertain; these fits therefore were not used for modeling (nor are they plotted in Figure 7). See text for further details.

AS	M-cone target (L-cone equated)				L-cone target			
Background wavelength	$\hat{s}$	*SE*	Δt	*SE*	$\hat{s}$	*SE*	Δt	*SE*
410 nm								
B	0.34	0.01	38.47	0.49	−0.16	0.02	24.96	1.36
469 nm								
B	0.81	0.02	26.95	0.16	−0.34	0.01	25.62	0.58
520 nm								
C	0.50	0.00	33.33	0.35	−0.19	0.02	27.68	1.21
578 nm								
C	0.45	0.00	31.23	0.12	−0.26	0.02	26.31	0.82
600 nm								
C	−0.50	0.01	22.31	0.40	0.24	0.01	21.40	0.56
658 nm								
B	−0.71	0.01	31.48	0.28	0.24	0.01	31.64	0.73
C	−0.74	0.02	22.72	0.28	0.33	0.01	21.60	0.30
D	0.57	0.00	29.50	0.10	−0.29	0.01	25.08	0.71

Table A8. Fits of the time-delay model to the data for AS. See text for further details.

Downloaded From: http://jov.arvojournals.org/pdfaccess.ashx?url=/data/journals/jov/936743/ on 02/20/2018